China Geology 6 (2023) 338−357

China Geology

Journal homepage: http://chinageology.cgs.cn
https://www.sciencedirect.com/journal/china-geology

Geology, geochronology, and exploration of the Jiama giant porphyry copper deposit (11 Mt), Tibet, China: A review

Bin Lin[a, b,*], Ju-xing Tang[a], Pan Tang[c,*], Wen-bao Zheng[a], Yang Song[a], Fa-qiao Li[b], Qiu-feng Leng[d], Zhi-chao Wang[e], Jing Qi[e], Miao Sun[e], Juan David Bello Rodríguez[b]

[a] *MNR Key Laboratory of Metallogeny and Mineral Assessment, Institute of Mineral Resources, Chinese Academy of Geological Sciences, Beijing* 100037, *China*
[b] *Department of Geology and Geological Engineering, University Laval, QC G1V* 0A6, *Canada*
[c] *The Key Laboratory of the Ministry of Education on Solid Waste Treatment and Recycling, School of Environment and Resource, Southwest University of Science and Technology, Mianyang* 621010, *China*
[d] *Chengdu Center, China Geological Survey, Chengdu* 610081, *China*
[e] *School of Earth Science and Resources, China University of Geosciences (Beijing), Beijing* 100083, *China*

ARTICLE INFO

Article history:
Received 1 March 2023
Received in revised form 5 April 2023
Accepted 6 April 2023
Available online 23 April 2023

Keywords:
Copper deposit
Porphyry copper system
O-S-Pb isotope
Multicenter complex mineralization
Comprehensive exploration model
Mineral exploration engineering
Gangdese metallogenic belt
Jiama
Tibet

ABSTRACT

Jiama, with more than 11 Mt of copper metal, is the largest porphyry-skarn copper system in the Gangdese metallogenic belt, Tibet, China, creating ideal conditions for deciphering the origin of porphyry ores in a collision setting. Despite massive studies of the geology, chronology, petrogenesis, and ore-related fluids and their sources in Jiama, there is a lack of systematic summaries and reviews of this system. In contrast to traditional porphyry copper systems in a subduction setting, recent studies and exploration suggest that the Jiama deposit includes porphyry-type Mo-Cu, skarn-type Cu polymetallic, vein-type Au and manto orebodies. This paper reviews the latest studies on the geology, chronology, petrogenesis, fluid inclusions, and isotopic geochemistry (hydrogen, oxygen, sulfur, and lead) of the Jiama deposit. Accordingly, a multi-center complex mineralization model was constructed, indicating that multi-phase intrusions from the same magma reservoir can form multiple hydrothermal centers. These centers are mutually independent and form various orebodies or are superimposed on each other and form thick, high-grade orebodies. Finally, a new comprehensive exploration model was established for the Jiama porphyry copper system. Both models established in this study help to refine the theories on continental-collision metallogeny and porphyry copper systems.

1. Introduction

The Jiama giant porphyry Cu polymetallic system is located in the southern Qinghai-Tibet Plateau, in the northern part of the Yarlung Zangbo suture zone, and at the southern margin of the Lhasa terrane (Tang JX et al., 2010, 2012; Zheng WB et al., 2016; Lin B et al., 2019). Geographically, the Jiama project, consisting of the Jiama mining project and the Jiama peripheral exploration project, lies in Mozhugongka County in the eastern part of Lhasa City. Before 1949, local residents mined lead ore in this area using indigenous methods, leaving behind two old tunnels in the region. In the 1950s, the Tibetan Geological Working Team (TGWT) determined that the Jiama project was a pyrometasomatic deposit dominated by Cu, Pb and Zn based on a 1∶25000 geological survey and revealed that the orebodies in this project primarily occurred in contact with limestones and slates (a technical report prepared by the No. 6 Geological Team of Tibet, unpublished). From 1956 to 2006, several geological survey teams from the Tibet Autonomous Region Geological and Mineral Exploration and Development Bureau successively carried out further explorations of the Jiama project, including field geological surveys, trenching, drilling, geophysical surveys, and soil/rock geochemical surveys (Du GS et al., 1998; Tang JX et al., 2010; Zheng WB et al., 2016). As a result, they revealed the mineralization and alteration of the project, determining that this project was a skarn-type

First author: *E-mail address*: linbincags@126.com (Bin Lin).
* Corresponding author: *E-mail address*: linbincags@126.com (Bin Lin); tangpan168@163.com (Pan Tang).

Literary editor: Xi-jie Chen
doi:10.31035/cg2023031
2096-5192/© 2023 China Geology Editorial Office.

deposit and might have the prospecting potential of a porphyry metallogenic system (Li GM et al., 2005; She HQ et al., 2005, 2006). During this period, some researchers believed that the Jiama project was a submarine sedimentary exhalative (SEDEX) deposit according to its orebodies and ore structures (Yao P et al., 2006). However, due to the limitations of the exploration level and theoretical research, no breakthrough has been achieved in the prospecting of the Jiama project. As of July 2007, only 1×10^5 t of inferred Cu and 2.262×10^5 t of Pb had been discovered in the main zone of the Jiama project (a technical report from the No. 6 Geological Team of Tibet, unpublished).

From 2007 to 2008, the China National Gold Group Co., Ltd. completed its purchase of the whole Jiama project and established Tibet Huatailong Mining Development Co., Ltd. (HTLM) for the economic exploration of the project (Zheng WB et al., 2016), Then, the HTLM invited a joint technical team from the Institute of Mineral Resources of the Chinese Academy of Geological Sciences and the Chengdu University of Technology to carry out systematic geological mapping, structural interpretation, and geophysical and geochemical surveys of the whole Jiama project under the supervision of professors Tang Ju-xing and Wang Deng-hong. Based on the obtained results, the technical team deployed an important borehole, ZK1616, in the middle part of the project after detailed geological surveys and interpretations of geochemical and geophysical anomalies (Tang JX et al., 2010; Zheng WB et al., 2016). Consequently, the discovery of high-grade, thick (about 252 m), skarn-type Cu polymetallic orebodies in the deep part started the large-scale economic exploration of the Jiama deposit (Zheng WB et al., 2016). Subsequently, more than 380 boreholes were drilled in the Jiama area. A total of approximately 200 km of core samples obtained from these boreholes revealed skarn-type Cu polymetallic orebodies, hornfels-type Cu-Mo orebodies, porphyry-type Mo-Cu orebodies and independent gold orebodies in the Jiama project (Lin B et al., 2019). The "four-in-one" orebody structure clearly indicates that the Jiama project is a porphyry system (Tang JX et al., 2010).

Since 2014, based on the continuous instructions and efforts from the exploration technical team, a new round of exploration of the deep and peripheral areas has been further carried out in the Jiama project. As a result, high-grade, thick, and large Cu (Au) orebodies have been discovered in various deep regions, further enhancing the economic value of the Jiama deposit. A huge porphyry Cu-Mo orebody with a thickness of more than 700 m has been encountered in the northeastern North-Zegulang zone during the drilling of new borehole ZK836 in the zone (Lin B et al., 2019). Its mineralization and alteration characteristics suggest the presence of an independent metallogenic hydrothermal center. Based on a systematic summary of the exploration and geological characteristics of the Jiama project, Lin B et al. (2019) defined a multi-center complex mineralization model for the Jiama porphyry system, thus further enriching and enhancing the metallogeny and exploration of porphyry copper deposits in the Qinghai-Tibet Plateau. By the end of 2022, the Jiama project had witnessed the discovery of over 11×10^6 tons of Cu, over 1.07×10^6 t of Mo, 1.75×10^6 t of Pb and Zn, 305 t of associated Au, and 15840 t of associated Ag, making it a world-class giant deposit (a technical report from the Tibet Huatailong Mining Development Co., Ltd., unpublished).

Since the discovery of the Jiama deposit, many geologists have carried out detailed studies on the geology, structure, magmatism, chronology, mineralogy, ore-forming fluids, stable isotopes, and exploration of the deposit (Tang JX et al., 2010; Zheng WB et al., 2016; Tang P et al., 2017; Wang YY et al., 2017; Lin B et al., 2012, 2019; Zheng SJ et al., 2021; Sun F et al., 2022). These studies have further promoted the economic exploration of the Jiama project. However, given the continuous exploration of the Jiama deposit, there is an urgent need to conduct a systematic summary and review of these studies. As a representative deposit formed in a continental collision environment, the Jiama deposit not only exhibits the general characteristics of a collision-related porphyry Cu system (Hou ZQ et al., 2015; Yang ZM et al., 2016) but also displays many unique features, such as high-grade orebodies and extensive gold mineralization. Consequently, based on the results obtained from a decade of exploration and research on the Jiama project, this paper provides a comprehensive overview of the geology, mineralization, and alteration of the Jiama porphyry ore system and further refines its mineralization and exploration models. This review will help improve porphyry metallogeny and continental collision metallogeny (Hou ZQ et al., 2010) and provide a scientific reference for the exploration of the porphyry systems in the Qinghai-Tibet Plateau.

2. Regional geology

Multi-stage subduction-collision processes not only enriched the geological structure of the complex orogenic belts on the Qinghai-Tibet Plateau but also created a favorable geological background for regional multi-style mineralization in the plateau (Lin B et al., 2017; Tang JX, 2019). The Qinghai-Tibet Plateau can be divided into the Himalayas, the Lhasa terrane, and the Qiangtang terrane from south to north with the Yarlung Zangbo and Bangongco-Nujiang suture zones as their boundaries (Lin B et al., 2019, 2021, 2022; Pan GT et al., 2006; Yin A, 2000). The Lhasa terrane is located in the central part of the Qinghai-Tibet Plateau, and its strata consist of the basements of the Paleoproterozoic-Mesoproterozoic Gangdese and Nyainqentanglha groups, as well as the overlying Paleozoic marine clastics, carbonate rocks, and local bimodal volcanic rocks and Mesozoic-Cenozoic extremely thick arc volcanic rocks, carbonate rocks, and clastics. The typical arc volcanic rocks in the Lhasa terrane were first formed in the Carboniferous strata, representing the transformation of its tectonic system from a passive continental margin to an active continental margin, which evolved into a multi-island arc-basin system during the

Mesozoic (Pan GT et al., 2006). As an important part of the Gangdese metallogenic belt, the Mesozoic sedimentary clastics, carbonate rocks, and volcanic rocks in the southern Lhasa terrane serve as the most important surrounding rocks for mineral deposits. Due to the continuous northward subduction of the Yarlung Zangbo Oceanic plate and the subsequent continental collision during the Mesozoic, a series of compressional thrust faults and folds formed in the southern Lhasa terrane, with multiple N-S-trending extension faults developing locally (Zhong KH et al., 2012).

In addition, large-scale volcanic and intrusive activities widely occurred in the southern Lhasa terrane. Volcanic activity primarily occurred during the Jurassic and Paleocene. As a result, mafic, intermediate, and felsic tuffaceous rocks (e.g., the Yeba and Xiongcun formations) were mainly formed during the Jurassic, while mafic, intermediate, and felsic rhyolite and tuffaceous rocks (the Linzizong Group) primarily occurred during the Paleocene. Intrusive activity mostly occurred during the Jurassic, Cretaceous, Paleogene, and Miocene. Accordingly, the Gangdese batholith was formed, including intermediate-felsic intrusions such as diorite, quartz diorite porphyry, monzogranite, and granite porphyry. As an important part of the Tethys-Himalayan metallogenic domain, the Gangdese metallogenic belt in Tibet is mainly distributed along the southern margin of the Lhasa terrane (Fig. 1a), with a length of about 600 km from east to west and a width of about 100 km (Tang JX et al., 2014a). This metallogenic belt hosts porphyry deposits, skarn deposits, and epithermal deposits (Fig. 1b) and consists mainly of (1) subduction-related porphyry-epithermal Cu-Au metallogenic systems related to the Yanshanian magmatism, such as Xiongcun and Dongga (Lang XH et al., 2014; Tang JX et al., 2015) and (2) post-collisional porphyry-skarn Cu-Mo polymetallic systems related to the Himalayan magmatism, such as Jiama, Qulong, Bangpu, Tinggong, and Zhunuo (Yang ZM et al., 2009; Tang JX et al., 2014b; Wang R et al., 2018; Tang P et al., 2021).

3. Deposit geology

The Jiama deposit is located in the eastern Gangdese metallogenic belt, the southern Lhasa terrane and the northern Yarlung Zangbo suture (Fig. 1b). The Jiama project features relatively simple exposed strata, namely the Upper Jurassic Duodigou Formation (J_3d), the Lower Cretaceous Linbuzong Formation (K_1l), and Quaternary strata in chronological order from oldest to youngest. Among them, J_3d consists of gray massive crystalline limestones and marbles, as well as thinly laminated slates, siltstones, and sandstones, which were all deposited in the platform-margin reef facies. Its thickness varies widely in the range of about 196–1741 m. K_1l is composed primarily of grayish-black carbonaceous slates and siltstones, quartz sandstones, and a minor quantity of pyrites and pyrrhotites, with a thickness of 112–1495 m. As residual deposits, the Quaternary strata are distributed along valleys and river valleys locally (Fig. 2; Lin B et al., 2019). Based on the present mining project and the latest exploration, the Jiama mining project of the Jiama project can be further divided into three ore zones, namely the main zone, the Copper Mountain (also named the South Pit) zone, and the North-Zegulang zone (Lin B et al., 2019).

The Jiama deposit is mainly controlled by the Jiama-Kajunguo thrust system (Zhong KH et al., 2012), which primarily refers to the "contracting" folds extending from north to south within the Jiama project and plays a crucial role in the formation of the No. 1 skarn orebody in Jiama. The Copper Mountain slip fault is an important part of the entire Jiama-Kajunguo thrust system and primarily refers to the Copper Mountain area in southeastern Jiama (Fig. 3). This major reverse slip fault is associated with several secondary folds and faults and controls the formation of the No. 2 skarn orebody in the Jiama project (Tang JX et al., 2017). In addition, detailed structural and alteration mapping reveals that the spatial locations of skarn alterations in the project are related to the secondary folding (D2) in the area (Duan JL et al., 2014). The secondary folding formed fractures and folds and led to the collapse between different rocks, thus providing abundant spaces for fluid migration and deposition. Accordingly, high-grade and thick skarn-type Cu polymetallic orebodies were formed. The mineralization of porphyry and hornfels is closely related to the fissure system formed by porphyry emplacement. The intermediate-felsic intrusions

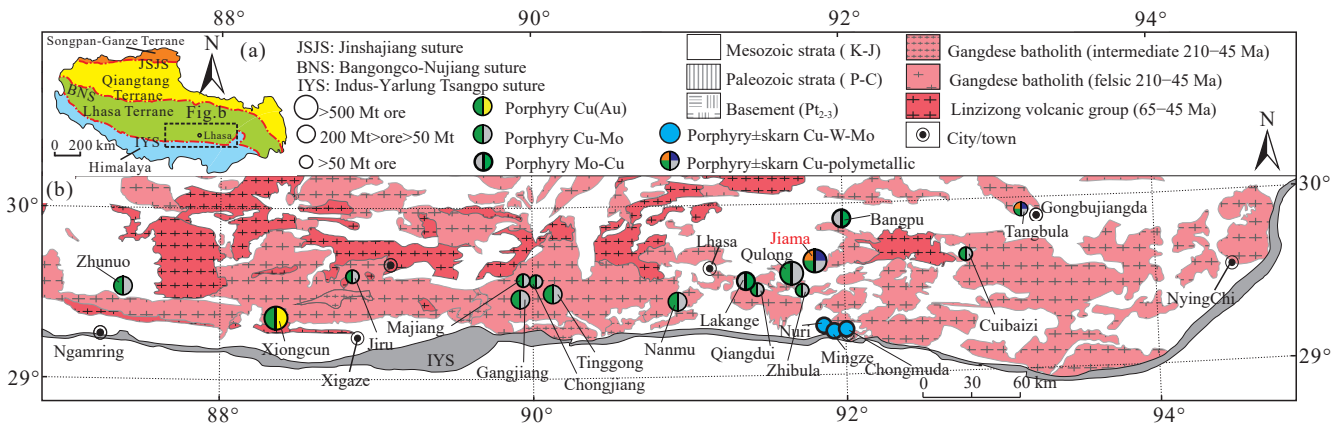

Fig. 1. Tectonic setting and regional geology of the Gangdese metallogenic belt in Tibet (modified from 1∶1500000 Tibetan Geological Map).

Fig. 2. Geology of the Jiama deposit showing the distribution of metal mineralization (modified from Lin B et al., 2019). 1–Quaternary sediment; 2–Sandstone, slate, and hornfels of the Lower Cretaceous Linbuzong Formation; 3–Limestone and marble of the Upper Jurassic Duodigou Formation; 4–Skarnized marble; 5–Skarn; 6–Skarn orebody; 7–Granite porphyry dike; 8–Granodiorite porphyry dike; 9–Quartz–diorite porphyry dike; 10–Aplite dike; 11–Slip fault; 12–Range of different ore zone; 13–Borehole and section

would supply heat to the overlying surrounding rocks, thus forming hornfels and marble alterations. This process was affected by the pressure shift during the fluid evolution. When the fluid pressure exceeded the lithostatic pressure exerted by the surrounding rocks, a wide range of fractures and fissures developed at the top of the porphyries and surrounding rocks and were subsequently filled with hydrothermal fluids, leading to the formation of ore-bearing veins.

The surface magmatic rocks in the Jiama project are relatively small and dominated by concealed, intermediate-felsic Miocene intrusions, with a small number of mafic dikes distributed locally. The intermediate-felsic intrusions include (quartz) diorite porphyry, granodiorite porphyry, monzogranite porphyry, granite porphyry, and a small number of aplite dikes in the main zone (Zheng et al., 2016). Among them, the monzogranite and granite porphyries are closely related to Mo mineralization, while the granodiorite porphyry and partial diorite porphyry are closely related to Cu mineralization. The mafic dikes mainly include the dark lamprophyre and diabase at the periphery of the Jiama project, most of which are the products of post-mineralization magmatism (Qin ZP, 2013).

The paragenesis of these intermediate-felsic intrusions in the main zone has been clearly revealed by hundreds of drillings. One barren aplite dike intruded into the Lead Mountain before the D2 deformation, forming a pre-mineralization intrusion (Duan JL et al., 2014). Then, the granite porphyry or monzogranite porphyry was emplaced. They consist of quartz, K-feldspar, plagioclase, and biotite phenocrysts, with almost no hornblende present, and their matrix is felsic. The monzogranite and granite porphyries are generally subjected to strong sericite and kaolinite alterations and weak biotite alteration. Many quartz-sulfide (molybdenite, chalcopyrite, and pyrite) veins occur in the

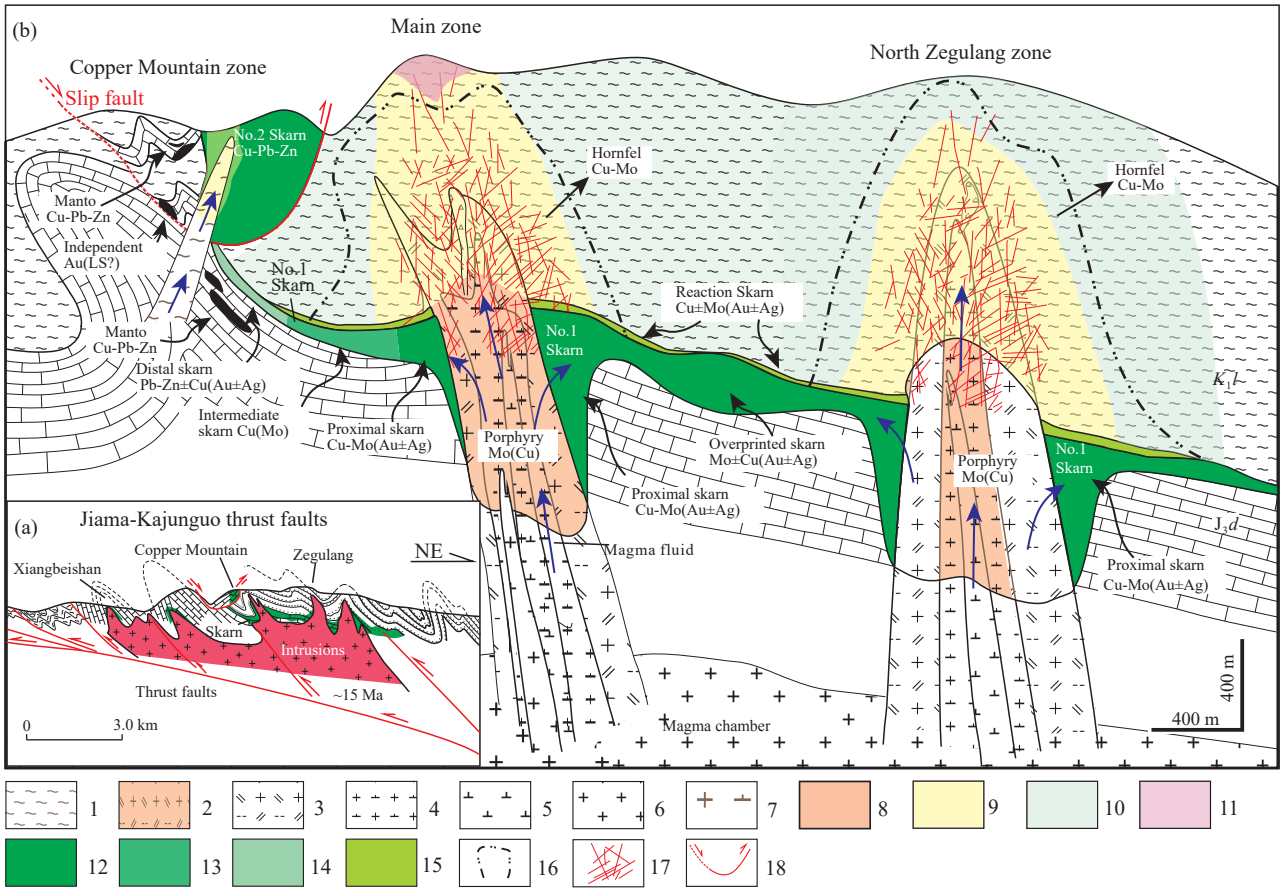

Fig. 3. Jiama-Kajunguo thrust fault system and the Jiama porphyry copper system (modified from Lin B et al., 2019). 1–Linbuzong Formation; 2–Duodigou Formation; 3–monzogranite porphyry; 4–granodiorite porphyry; 5–quartz diorite porphyry; 6– quartz monzonite porphyry; 7–breccia, 8–potassic alteration; 9–sericite alteration; 10–weak chlorite and epidote alterations; 11–silicate alteration; 12–proximal skarn; 13–intermidiate skarn; 14–distal skarn; 15–reaction skarn; 16–boundary of Cu-Mo orebody in hornfels; 17–veins and fissures; 18–slip fault.

monzogranite and granite porphyries, leading to typical porphyry Mo-Cu mineralization. The granodiorite porphyry intruded later, forming cross-cutting relationships with the monzogranite and granite porphyries. Compared to the monzogranite and granite porphyries, the granodiorite porphyry hosts larger quantities of quartz, hornblende, and plagioclase phenocrysts and a smaller amount of biotite phenocrysts. The hornblende, plagioclase, and biotite phenocrysts in the granodiorite porphyry are usually subjected to chlorite alteration. Skarn alteration occurs in the granodiorite porphyry and its contact with marble, forming endoskarn and proximal skarn, respectively. The granodiorite porphyry generally hosts disseminated chalcopyrite and pyrite, as well as quartz-chalcopyrite-pyrite-molybdenite veins. Subsequently, quartz diorite porphyry or diorite porphyry intruded and cuts the monzogranite and granodiorite porphyries. The quartz diorite porphyry consists of many fine-grained plagioclase and hornblende phenocrysts and a small quantity of quartz phenocrysts. Chlorite and sericite alterations also occur in the plagioclase and hornblende phenocrysts within the quartz diorite porphyry, which contains a small amount of disseminated pyrite and chalcopyrite, as well as local quartz-pyrite-chalcopyrite veins. The latest intrusions include the newly identified quartz monzonite porphyry and some fine-grained granite aplite dikes, which are only emplaced locally. The quartz monzonite porphyry contains a small quantity of quartz, plagioclase, K-feldspar, and biotite phenocrysts and exhibits extensive sericite alteration. The granite aplite dikes are composed of abundant fine-grained quartz and a small amount of biotite and plagioclase. These dikes host almost no sulfide and a small number of quartz veinlets locally, representing the post-mineralization magmatism.

4. Mineralization and alterations

The geological alteration and mineralization features of the main orebodies in various ore zones are stated as follows.

4.1. Main zone

The main zone, located in the central part of the Jiama project, mainly hosts the No. 1 skarn orebody in the interlayer detachment zone, the top hornfels-type orebody, and the deep porphyry-type orebody. The No. 1 skarn orebody has a nearly NW-SE strike and a NE trend, along which it extends for about 2 km and about 3 km, respectively (Fig. 4). Its NE extension has not yet controlled its boundary. This orebody is generally laminated and thick-plate-like and occurs in the detachment zone between the Duodigou and Linbuzong formations. The shallow part of this orebody is primarily

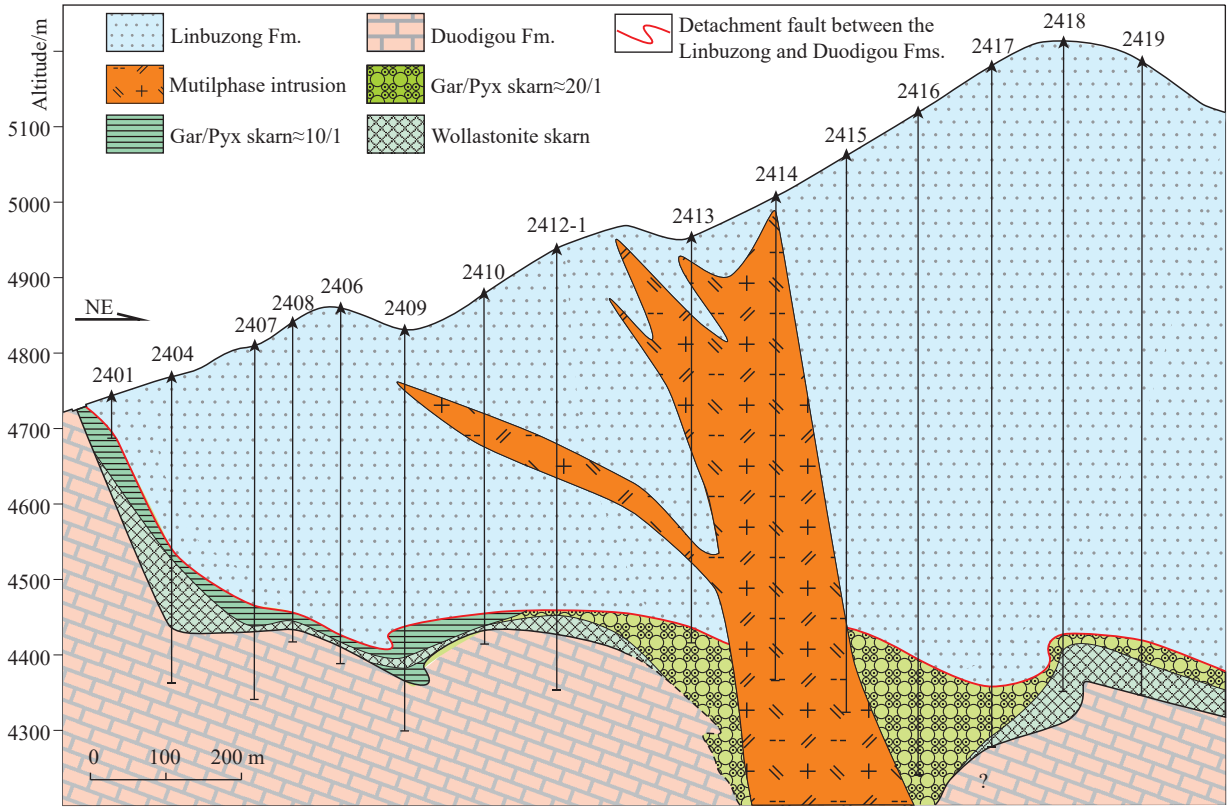

Fig. 4. No. 24 geological section and the distribution of skarn minerals in the Jiama deposit (modified from Zheng WB et al., 2016).

subjected to Pb-Zn mineralization, while its deep part mainly exhibits Cu-Mo mineralization and gold (Au) and silver (Ag) mineralization (Figs. 2, 3). The ores are mostly disseminated, massive, and small veined (Fig. 5a, b). The major metal minerals in the No. 1 skarn orebody include chalcopyrite, bornite, molybdenite, pyrite, galena, sphalerite, magnetite, pyrrhotite, digenite, tetrahedrite, chalcocite, covellite, specularite, Au-Ag minerals, and a small amount of scheelite, cobaltite, and bismuth-bearing minerals (e.g., cooperite, bismuthite, bismuth antimonate, and bismuth-bearing tetrahedrite and bornite; Fig. 6; Lin B et al., 2019; Ying LJ et al., 2010). Gangue minerals in the orebody mainly include garnet, diopside, wollastonite, tremolite, hornblende, chlorite, epidote, quartz, calcite, anhydrite, and a small amount of fluorite. In the horizontal direction, the skarns in the orebody present significant mineral zoning, including garnet skarn, diopside garnet skarn, garnet diopside skarn, and garnet wollastonite skarn from the inner intrusions outward, with the ratio of garnet to pyroxene ranging from 20∶1 to 10∶1 and then to 51 and the garnet color varying from reddish-brown to brownish-green and then to pale-yellow (Zheng WB et al., 2016; Leng QF et al., 2015, 2022). The ratio of andradite to grossular garnet in the garnet composition decreases gradually as well. The corresponding metal mineralization and mineralizing elements also exhibit distinct zoning. From the inner outward, molybdenite (chalcopyrite-bornite) transitions to chalcopyrite-bornite-molybdenite and then to galena-sphalerite-chalcopyrite-bornite (molybdenite), and the major mineralizing elements change from Mo (Cu, Au, Ag) to Cu-Mo-Au-Ag and then to Pb-Zn-Cu-Au-Ag (Zheng WB et al., 2016). In the vertical direction, the skarns also show significant mineral zoning and mineralization zoning. Specifically, the skarns at the top and nearby the hornfels are dominated by garnet skarn, and the mineralization is dominated by rich chalcopyrite and molybdenite mineralization; the middle part hosts diopside garnet skarn and shows the mineralization of chalcopyrite, molybdenite, bornite, and a small amount of galena and sphalerite; and the bottom near the marble mainly develop garnet wollastonite skarn and develops bornite and chalcopyrite mineralization.

Porphyry mineralization occurs in two types of orebodies hosted in porphyries and hornfels. The hornfels-hosted orebodies occur in the surrounding rocks at the top of multiple intrusions and are mainly controlled by magmatic-hydrothermal alteration. These orebodies each have a width of more than 2 km and a thickness of 0.9 km (Lin B et al., 2019), mainly exhibiting disseminated and stockwork Cu-Mo mineralization (Figs. 5c, d). Their metal minerals include pyrite, chalcopyrite, molybdenite, magnetite, pyrrhotite, and a small amount of bornite (Fig. 6), while their gangue minerals primarily consist of quartz, plagioclase, biotite, chlorite, epidote, sericite, calcite, tourmaline, anhydrite, garnet, and diopside. Regarding the alterations of the hornfels-hosted orebodies, they primarily involve strong silicification, biotite and sericite alterations and local chlorite, epidote, garnet, and tourmaline alterations as follows: (1) The strong silicification mainly refers to the formation of silicate hornfels by heating and metamorphism, as well as the formation of numerous quartz-sulfide veins; (2) The biotite alteration includes the change from feldspar components in rocks to fine-grained,

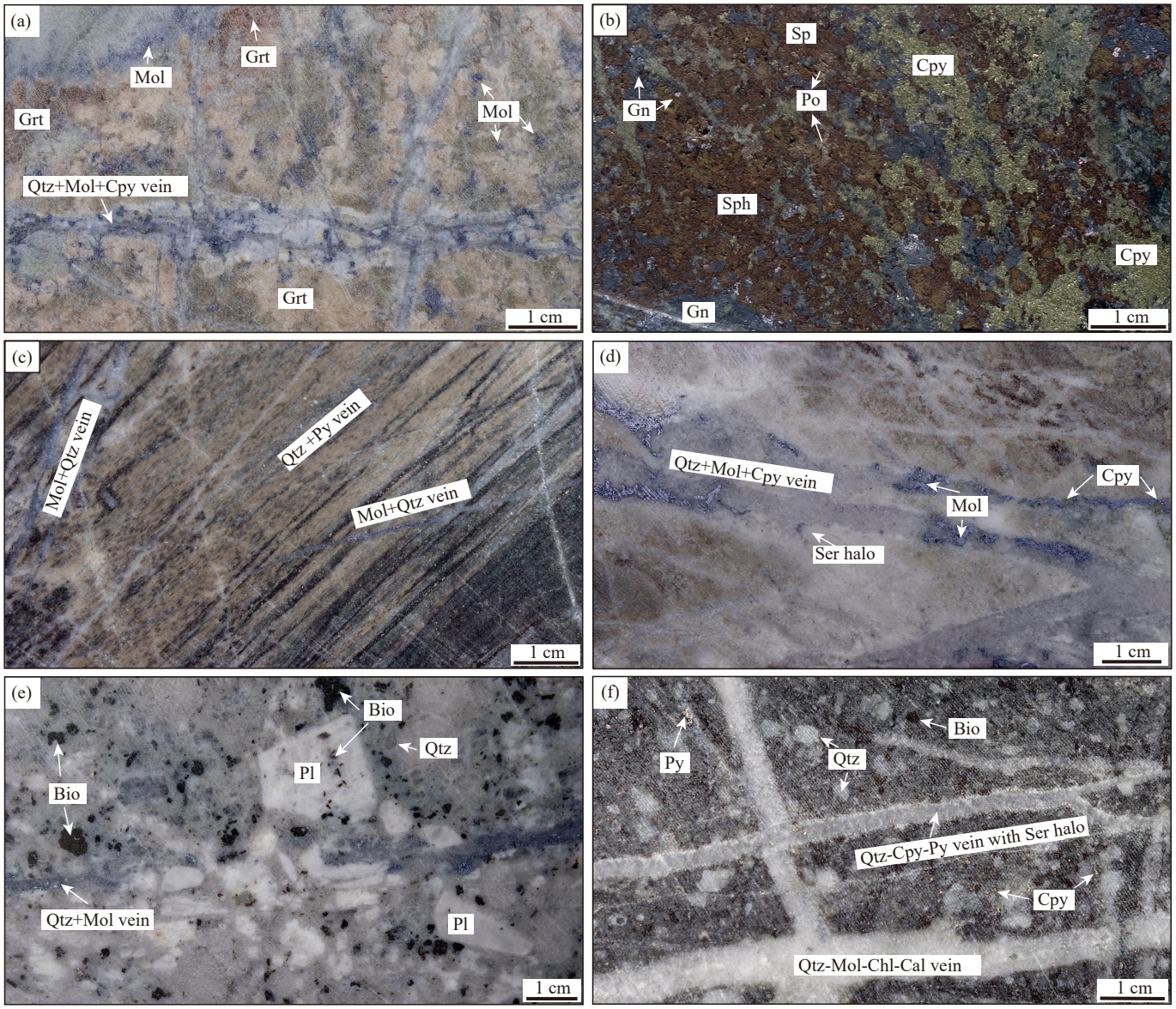

Fig. 5. Mineralization in different host rocks in the Jiama deposit, Tibet. a–Veins and disseminated Mol and Cpy in skarn; b–Massive Sph-Cpy-Gn-Po in the skarn; c–Qtz-Mol and Qtz-Py veinlets in hornfels; d–Qtz-Mol-Cpy veins with Ser halos in hornfels; e–Qtz-Mol veins in the porphyry; f–Qtz-Mol-Chl-Cal veins cut by Qtz-Cpy-Py veins with Ser halos in the porphyry. Bio–biotite; Cpy–-chalcopyrite; Chl–chlorite; Grt–garnet; Gn–galena; Mol–molybdenite; Pl–Plagioclase; Po–pyrrhotite; Py–pyrite; Qtz–quartz; Ser–sericite.

banded or spotted biotite (including hydrothermal biotite veins); (3) The extensive sericite alteration can superimpose the silicate and biotite alterations caused by hydrothermal fluids, forming pervasive sericite alteration or halos of quartz-sulfide veins; (4) The chlorite and epidote alterations mainly consist of veined and pervasive alterations at the bottom of hornfels, forming chlorite-bearing quartz-sulfide veins or chlorite veins; (5) The garnet and diopside alterations mainly occur at the bottom of hornfels as veined, patchy, or irregular alterations and are typical skarn alterations; (6) The tourmaline appears as hydrothermal veins locally. The hornfels-hosted orebodies exhibit the mineralization of disseminated and veined chalcopyrite, pyrite, molybdenite, and a small amount of pyrrhotite. The veins in the hornfels-hosted orebodies are of the B and D types. The B-type veins primarily include quartz-pyrite-chalcopyrite and quartz-molybdenite veins. They mostly have a width of more than 5 mm and straight edges, extending for over 5 m. Sericite alteration halos occur on both sides of the B-type veins, and chlorite, biotite, tourmaline, and calcite develop in parts of these veins. The D-type veins are predominantly pyrite-chalcopyrite veinlets, with a width of above 3 mm. They can extend for more than 1 m, with sericite and chlorite halos visible locally.

The porphyry-hosted orebodies mainly occur at the top of multiple intrusions in the middle part of the main zone (boreholes Nos. 1216–3216; Lin B et al., 2012). Currently, these orebodies have not been completely controlled. The ores in these orebodies primarily include quartz-sulfide veins, some of which are disseminated (Figs. 5e, f). Dominating metal minerals in the ores are molybdenite, chalcopyrite, pyrite, and a small amount of bornite (Fig. 6). The gangue

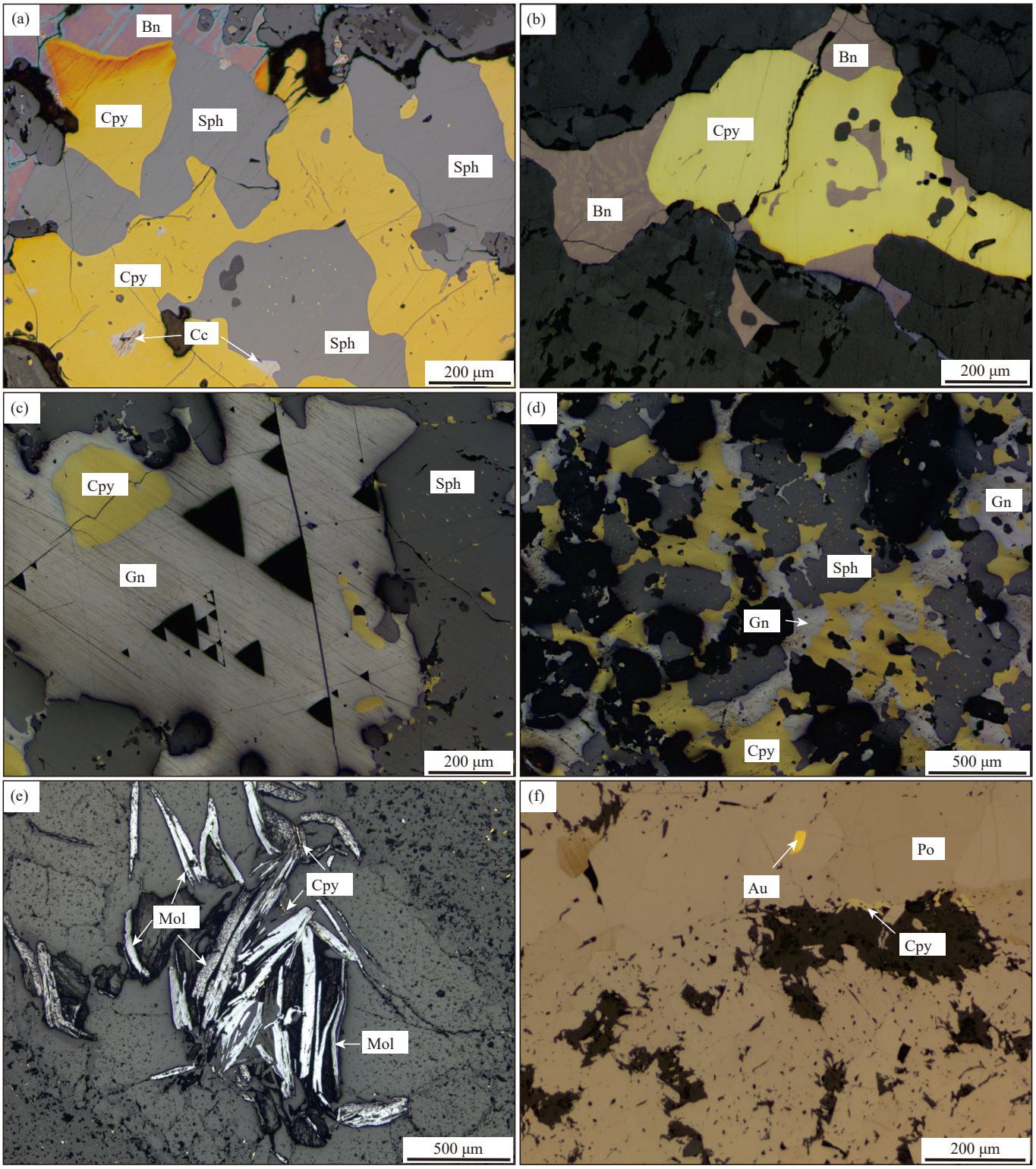

Fig. 6. Photomicrographs of different types of mineralization in the Jiama deposit, Tibet. a–Cpy, Sph, Cc and Bn mineralization in skarn; b–Bn and Cpy mineralization in skarn; c–d–Cpy, Gn, and Sph mineralization; e–Mol and Cpy mineralization in porphyry; f–Au in the Po with Cpy in skarn. Au–electrum; Bn–bornite; Cc–chalcocite; Cpy–chalcopyrite; Gn–galena; Mol–molybdenite; Po–pyrrhotite; Sph–Sphalerite.

minerals in the ores mainly include quartz, plagioclase, hornblende, biotite, calcite, and a small amount of anhydrite. The ore-hosting porphyries exhibit pervasive alterations, including weak potassium-sodium-silicate alteration, sericite alteration, and weak chlorite alteration. From the inside outward, the cores show relatively fresh porphyry (unaltered barren cores), weak alterations of potassium-sodium silicate (e.g., biotite, K-feldspar, and albite) and chlorite, and extensively superimposed sericite in sequence. These porphyries host several types of veins, namely A-, EB-, B-, and D-type veins. The A-type veins primarily consist of barren quartz veinlets and minor quartz-molybdenite veinlets, which typically have a narrow width of less than 5 mm and curved edges and extend continuously for less than 20 cm. K-

feldspar and albite alterations occur as the halos of these veinlets locally. The EB-type veins mainly refer to minor biotite veinlets, which primarily include hydrothermal biotite. These veins mostly have a width of less than 5 mm and curved edges and extend continuously for up to 50 cm. These veins may have albite and sericite alteration halos at their edges and almost bear no sulfides. The B-type veins are dominated by quartz-molybdenite veins, with some of them containing a small amount of hydrothermal biotite, chalcopyrite, pyrite, and anhydrite. These veins mostly have a width of over 5 mm and relatively straight edges and extend for more than 1 m. Sericite alteration halos are visible on both sides of some of these veins. The D-type veins are quartz-calcite-pyrite-chalcopyrite veins, with straight edges and high continuity, mostly extending for more than 1 m. Distinct sericite or chlorite alteration halos are visible on both sides of the D-type veins.

Several veined gold orebodies occur in the quartz diorite porphyry dike in the northwest Niumatang area, as revealed by boreholes such as No. 4504. They have a length of about 100 m and a width of 10–13 m and are mainly present as quartz-sulfide veins. These sulfides mainly include pyrite, arsenopyrite, calcite, and limonite (Fig. 2; Zheng WB et al., 2012).

4.2. Copper Mountain zone

The Copper Mountain zone is located in the south of the Jiama project and hosts the No. 2 skarn orebody (Fig. 7a; Zou B et al., 2019), which is controlled by the Copper Mountain slip fault and is present as a thick plate (Zhong KH et al., 2012). The No. 2 skarn orebody has a nearly-NW-SE strike and a NE trend, along which it extends for about 1000 m and more than 700 m, respectively. This orebody shows high-grade Cu-Pb-Zn mineralization and contains massive skarns. The metal minerals of this orebody include pyrite, chalcopyrite, galena, sphalerite, and a small amount of molybdenite, pyrrhotite, magnetite, specularite, Au-Ag minerals, and bismuthine. Its gangue minerals primarily include garnet, diopside, wollastonite, idocrase, tremolite, hornblende, chlorite, epidote, quartz, calcite, and gypsum. Compared with the No. 1 skarn orebody in the main ore segment, the No. 2 skarn orebody in the South Pit ore segment primarily exhibits Cu-Pb-Zn mineralization and relatively weak Mo mineralization. The No. 2 skarn orebody exhibits similar skarn mineral assemblages to the No. 1 skarn orebody, except for the weak mineral zoning. In addition, veined gold orebodies have been found in the skarns during the drilling of borehole No. ZK8806, showing strong silicate alteration and being enriched in sulfides, such as pyrrhotite and pyrite (Fig. 5). The gold mineralization is closely related to bismuth minerals. Sulfides, including chalcopyrite, sphalerite, galena, bornite and pyrrhotite, occur as veins and assemblages in fractures or deformation zones. They are accompanied by weak silicate alteration and quartz-calcite veins as the product of fluid escape, forming high-grade manto-type orebodies (Tang JX et al., 2011; Tang P et al., 2017).

4.3. North Zegulang zone

The North-Zegulang zone is located in the northeast of the Jiama project. Several boreholes have been drilled in this zone to date, revealing thick porphyry-type Cu-Mo orebodies, hornfels-type Cu-Mo orebodies, and skarn-type Cu polymetallic orebodies. For instance, a thick porphyry-type Mo-Cu orebody with a thickness of about 750 m, an average copper grade of 0.2%, and an average molybdenum grade of 0.03% was encountered during the drilling of borehole ZK836 (Fig. 7B; Lin B et al., 2019). Recent explorations show that the orebodies in this zone have roughly the same mineral assemblages, mineralization, and alterations as those in the main ore segment. However, they are related to different intrusions and belong to different hydrothermal centers. Therefore, the north Zegulang ore segment has great prospecting potential and is the key area of the present exploration.

In addition, other areas outside the Jiama project, such as the Mogulang and Xiangbei mountains, might also be future exploration targets based on the geological, geochemical, and geophysical surveys (Lin B et al., 2019).

In combination with the characteristics of the mineral assemblages in different orebodies and the cross-cutting relationships of veins, it can be determined that the mineralization in the Jiama deposit-as a whole porphyry system-involves three important events, namely magmatism, the hydrothermal event, and the supergene event (Fig. 8; Leng QF, 2016). The magmatism in the deposit refers to the emplacement and crystallization of ore-related intermediate-felsic intrusions. The hydrothermal event includes the prograde and retrograde metamorphic stages during the formation of skarn, as well as different quartz-sulfide stages, the quartz-gold mineralization stages, and the quartz carbonate stage. The supergene event refers to the oxidation and secondary enrichment following the mineralization induced by surface secondary hydrothermal fluids or supergene fluids (atmospheric water).

5. Discussion

5.1. Geochronology of magmatism and the hydrothermal event

Great efforts have been made in the chronological study of the Jiama deposit since its discovery, determining that the magmatic-hydrothermal activity occurred at about 15 Ma. Du GS (1998) first conducted the chronological analysis of magmatism in the Jiama deposit, obtaining the ages of the granodiorite and granite porphyries in the project as 14.9 Ma and 13.4 Ma, respectively. Subsequently, Chung SL et al. (2003) determined the ages of two granite porphyries as 17.0 ± 0.5 Ma and 15.0 ± 0.4 Ma using SHRIMP U-Pb dating of zircons (Fig. 9). Based on the Ar-Ar chronology of many

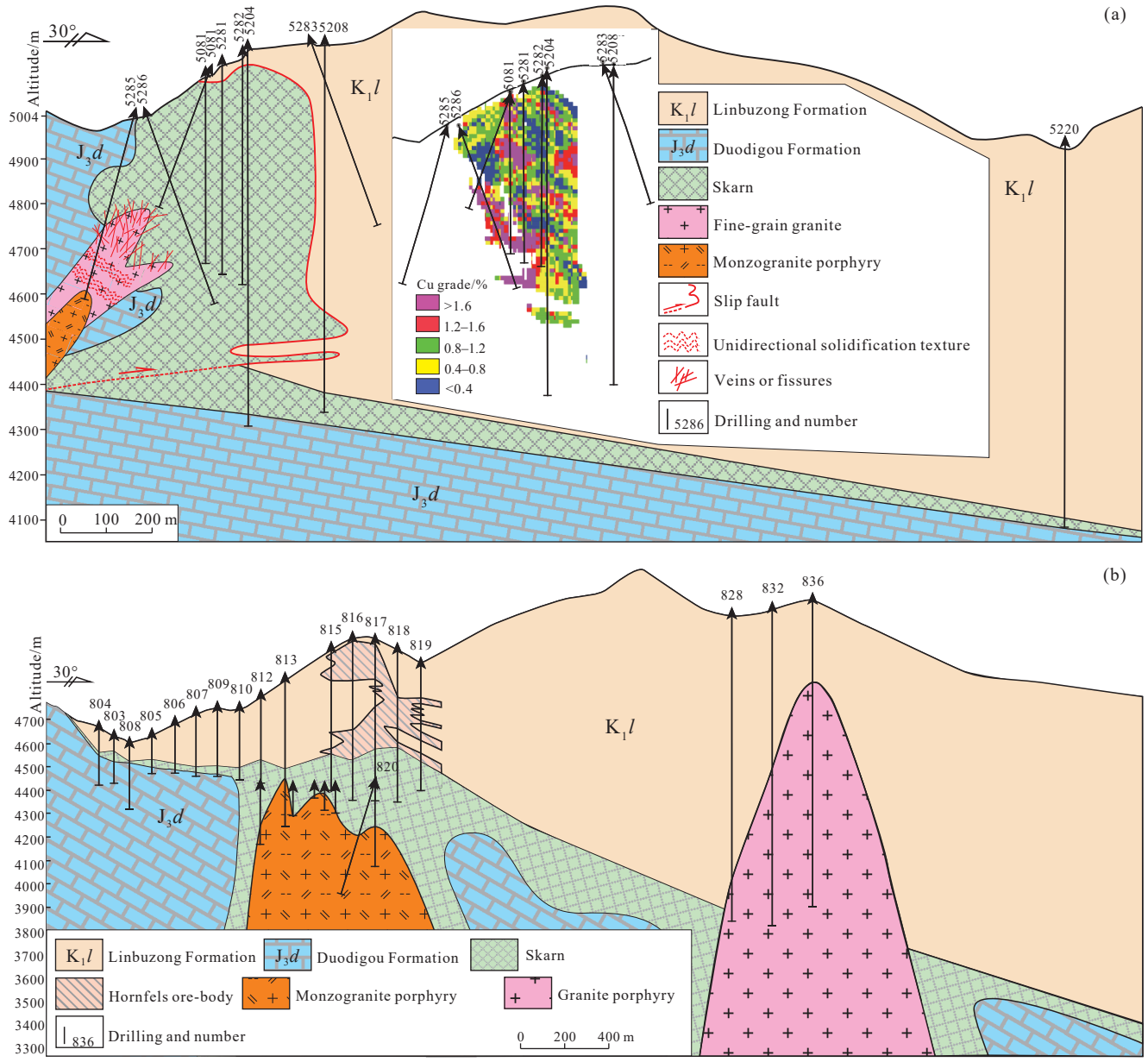

Fig. 7. Geology and mineralization of No. 52 (a) and No. 8 (b) geological sections in the Jiama deposit (modified from Lin B et al., 2019).

samples, it can be determined that the Jiama project has plateau ages of 15.2 ± 0.2 Ma and 13.2 ± 0.2 Ma (Fig. 9; Chung SL et al., 2003). Then, the geological mapping shows that the granite and monzogranite porphyries from the Xiangbei Mountain and the Talongwei, Dongfengya, and Dulifeng areas have LA-ICP-MS U-Pb ages of 16.1 ± 0.2 Ma, 16.0 ± 0.4 Ma, 14.8 ± 0.1 Ma, and 15.2 ± 0.3 Ma, respectively (Qin ZP et al., 2011). Ying LJ et al. (2011) completed detailed logging of the previously prospected No. 52 tunnel, discovering ore-bearing granite and granodiorite porphyries in the Lead Mountain, which have ages of 14.2 ± 0.2 Ma and 14.1 ± 0.1 Ma, respectively, according to the SHRIMP U-Pb dating of zircons.

Multiple phases of intermediate-felsic porphyries with different petrographic characteristics have been encountered in hundreds of boreholes in the Jiama project. The LA-ICP-MS zircon U-Pb dating shows that the granodiorite porphyry (DHH813–171.7 m) and the quartz diorite porphyry (DHH813–339.1 m) in the project have ages of 15.7 ± 0.1 Ma and 16.0 ± 0.1 Ma, respectively. Four monzogranite porphyry samples yielded similar U-Pb ages of 16.0 ± 0.1Ma (DHH2010–663.7 m), 15.6 ± 0.1 Ma (DHH813–605.2 m), and 15.5 ± 0.1 Ma (DHH2414–621.3 m) (Ying LJ, 2012; Zheng WB et al., 2016). In the Lead Mountain area, the early emplaced aplite was folded and deformed under the influence of later structures, with a U-Pb age of 16.9 ± 0.4 Ma (Duan JL et al., 2014). The diorite porphyry in the Niumatang area has an emplacement age of 14.0 ± 0.1 Ma (4504.0–188.5 m) (Fig. 9; Ying LJ, 2012). LA-ICP-MS zircon U-Pb dating shows that the ore-bearing granodiorite and granite porphyries in the Copper Mountain zone have zircon U-Pb ages of 14.8 ± 0.2 Ma (DHH5486–126.3 m) and 15.4 ± 0.5 Ma (DHH4280–345 m), respectively (Tang P et al., 2019; Zou B et al., 2019). In addition, LA-ICP-MS zircon U-Pb dating shows that the

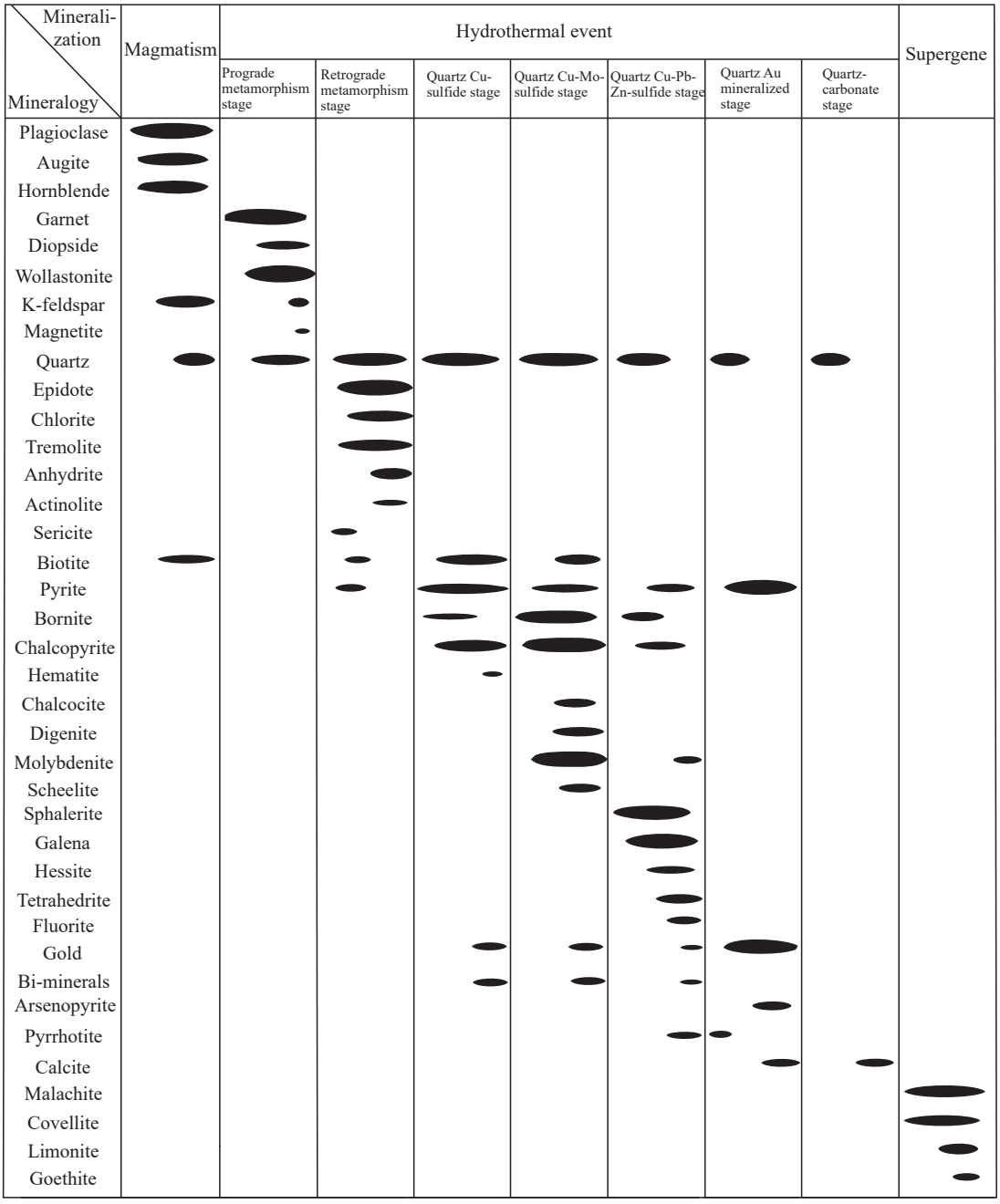

Fig. 8. Paragenesis of the mineralization in the Jiama deposit, Tibet (modified from Leng QF, 2016). *Note*: the width of the dark areas represents the contents of different minerals in different stages.

surface altered granite porphyry in the North-Zegulang zone has a zircon U-Pb age of 15.7 ± 0.3 Ma (Qi J et al., 2023). Sun et al. (2022) also conducted the SIMS U-Pb dating of zircons for the granite, diorite, and granodiorite porphyries in the Jiama project, obtaining ages of (16.19 ± 0.20–14.90 ± 0.16) Ma, 15.24 ± 0.17 Ma, and 15.44 ± 0.16 Ma, respectively.

Regarding the mineralization timing, Li GM et al. (2005) conducted Re-Os isotopic dating of molybdenite from the skarns in the Jiama project, obtaining an isochron age of 15.18 ± 0.98 Ma (Fig. 9). She HQ et al. (2005) also carried out Re-Os isotopic dating of seven molybdenite samples from the skarn, obtaining an isochron age of 15.70 ± 0.36 Ma. The two dating results are consistent within the error range. Ying LJ et al. (2009, 2010) conducted Re-Os isotopic dating of molybdenite from the disseminated molybdenite or quartz-molybdenite veins in the skarn, hornfels, and porphyry, obtaining isochrones ages of 15.34 ± 0.10 Ma (n = 10, MSWD = 0.85), 14.67 ± 0.19 Ma (n = 5, MSWD = 1.19), and 14.78 ± 0.33 Ma (n = 19, MSWD = 4.9), respectively. Tang P et al. (2019) carried out Re-Os isotopic dating of molybdenite from the No. 2 skarn orebody in the South Pit ore segment and obtained an isochron age of 15.2 ± 0.4 Ma (Fig. 9).

As shown by the above chronological studies, the magmatism in the Jiama project occurred during 17.0–14.1 Ma, with a span of about 2.9 Ma. It seems that the molybdenite in different ore-hosting rocks has different Re-Os ages. The molybdenite in skarn has been repeatedly

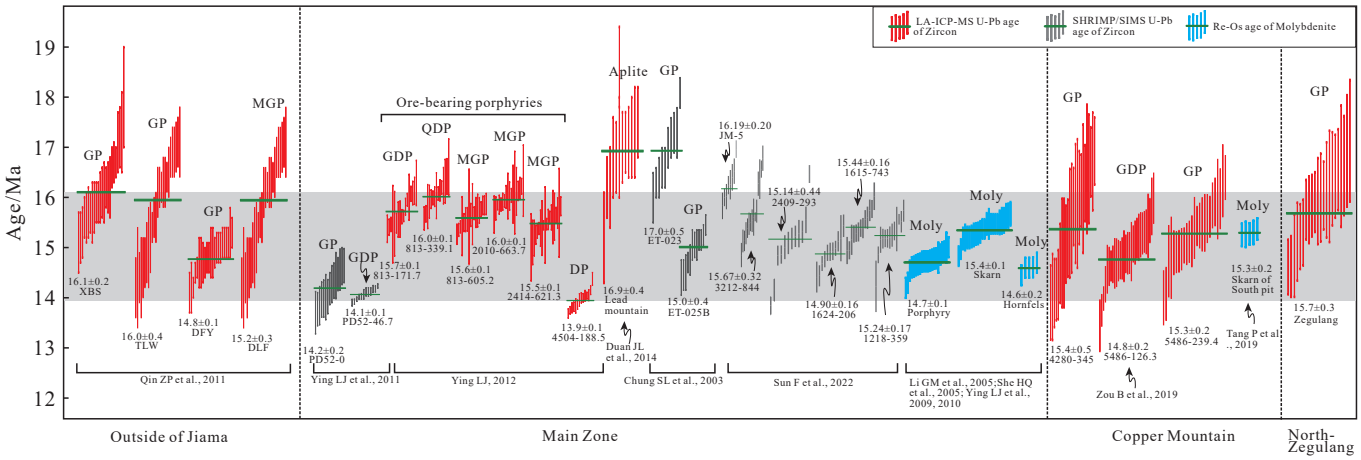

Fig. 9. Geochronology of the Jiama deposit, Tibet.

determined to have Re-Os isotopic ages of 15.70–15.18 Ma, while the veined molybdenite in hornfels and porphyries has slightly younger Re-Os ages of 14.67–14.78Ma (Fig. 9). The metallogenic ages of molybdenite in different types of ores are consistent with the magmatism time of the Jiama project within the error range. However, there are still several controversial questions, and the examples are as follows: (1) As mentioned above, multi-phase magmatic activities in the Jiama project spanned about 2.9 Ma. However, high-precision chronological studies of several large or giant porphyry metallogenic systems within the project reveal that, although magmatism might exhibit multi-phase characteristics, the ore-related magmatism has a duration of less than 1 Ma (Li Y et al., 2017; Large S et al., 2020). Therefore, it is necessary to conduct more detailed petrographic and chronological studies to obtain high-precision geochronological data of the ore-related magmatism in the Jiama project; (2) The current Re-Os ages of molybdenite in the Jiama project reveal that the molybdenite in skarn has slightly older isochron ages than that in hornfels and porphyries. The hydrothermal fluids in the skarn, hornfels, and porphyries in a unified porphyry copper system should have consistent precipitation times if the mineralization of the three types of host rocks was caused by the same type of magmatic-hydrothermal fluid at the same time. Presently, the Re-Os isotopic ages of molybdenite from different rock types differ by more than 0.7 Ma, which may be caused by different hydrothermal events or the decoupling in the Re-Os isotopic dating (Li C et al., 2009). Therefore, more efforts should be made to determine the exact mineralization time of the Jiama project and to carry out the Re-Os isotopic dating of molybdenite. Lin B et al. (2023) defined the pre-mineralization monzogranite (granite) porphyry, syn-mineralization granodiorite and quartz diorite porphyries, and post-mineralization quartz monzonite porphyry according to detailed logging and cross-cutting relationships. High-precision chemical abrasion-isotope dilution-thermal ionization mass spectrometry (CA-ID-TIMS) zircon U-Pb dating indicates that these porphyries have emplacement ages of 15.534 Ma, 15.368 Ma, 15.076 Ma, and 14.925 Ma, respectively, which constrain the duration of the ore-related magmatism to about 600 Kyr.

As shown by previous geochemical studies, the ore-bearing porphyries in the Jiama deposit are characterized by high SiO_2, Al_2O_3 and K_2O contents, high Sr/Y ratios, and a high affinity for adakites (Qin ZP et al., 2011, 2013; Zhang ZB et al., 2019; Sun F et al., 2022). These igneous rocks were remelted in the juvenile lower crust in a post-collisional setting, and their magmatic zircons have depleted Hf isotopic values *εHf(t)* of -0.9–4.6 and moderate $\delta^{18}O$ values varying from +5.21 to + 7.18‰ (Zhang ZB et al., 2019; Sun F et al., 2022). However, the evolutionary history of these ore-bearing porphyries is still controversial. Zhang ZB et al. (2019) argued that magma mixing and mingling occurred in the Jiama deposit, as evidenced by field observations, petrography, and geochemistry of the dioritic mafic microgranular enclaves (MMEs) in these porphyries. They emphasized insisted that the mixing of high-Mg dioritic MMEs plays a significant role in supplying water and metal materials to the felsic magmatic system, ultimately controlling the Cu polymetallic mineralization in the Jiama deposit. However, based on the geochemistry of whole rocks and the plagioclase and zircons from these ore-bearing porphyries, Sun F et al. (2022) proposed that there was no significant injection or mixing of mafic melts from different sources during the evolution of ore-related magmas. Therefore, it is necessary to carry out more detailed petrographic, in-situ geochemical, and isotopic studies to refine the petrogenesis of ore-related porphyries in the Jiama porphyry copper system.

In summary, the Jiama porphyry mineralization system is related to the Miocene (about 15 Ma) intermediate-felsic magmatic-hydrothermal event. Based on regional metallogeny and geochronology, it can be determined that the porphyry deposits in the Gangdese metallogenic belt, such as Qulong, Bangpu, Lakang'er, Junuo, Tinggong, Gangjiang, and Dabu, were all formed during the Miocene (17–13 Ma) and are related to intermediate-felsic high-K calc-alkaline magmas. They represent large-scale, regional Cu polymetallic mineralization events in a post-collisional setting (Yang ZM et al., 2009, 2019). Previous studies show that the porphyry Cu mineralization events in China occurred during the

Precambrian, Paleozoic, Mesozoic, and Cenozoic (Fig. 10). For instance, the Tongkuangyu porphyry copper deposit in the Paleoproterozoic Zhongtiaoshan orogenic belt represents the earliest porphyry Cu mineralization event in China (Meng XY et al., 2020); the Heersai, Mengxi, Duobaoshan, Bainaimiao, Tuwu-Yandong, and Baogutu deposits represent Paleozoic mineralization and are mostly distributed in the Central Asian Orogenic Belt; the Duolong, Xiongcun, Dexing, and Zijinshan deposits reflect the Mesozoic porphyry Cu mineralization and are widely distributed in different belts (Lin B et al., 2017, 2018, 2019, 2021; Yang ZM et al., 2019); the Yulong copper belt is the typical product of the Cenozoic Eocene porphyry mineralization and is related to the collisional orogeny of the Indian and Eurasian plates (Lin B et al., 2018); and the Gangdese metallogenic belt and the Qulong and Jiama deposits represent the latest porphyry Cu mineralization event (Fig. 10), which is, however, the largest regional mineralization event in the Gangdese metallogenic belt from the perspective of the deposit number and copper tonnage (Yang ZM et al., 2019).

5.2. Ore-forming fluids and sources

Yao P et al. (2006) investigated the characteristics of the rare earth elements and silicon isotopes of laminated skarns in the Jiama project and proposed that the ore-forming fluids of the project originated from hydrothermal fluids in ancient oceans. However, She HQ et al. (2006) measured the temperatures of fluid inclusions in various minerals, such as garnet, quartz, wollastonite, and calcite, in the Jiama deposit and discovered that the fluid inclusions in garnet were not uniform at 570°C. This result indicates that the ore-forming fluids of the project originated from high-temperature magmatic-hydrothermal fluids. The liquid-rich, vapor-rich, and daughter mineral-bearing inclusions in the quartz-molybdenite veins have homogenization temperatures of 201–443 °C, 384–467 °C, and 185–366 °C, respectively, suggesting that the ore-forming fluids are medium-high-temperature hydrothermal fluids. However, the salinity of these inclusions varies widely. The gas-liquid two-phase inclusions have salinities of 1.4%–11.7% $NaCl_{equ}$, while the inclusions bearing daughter crystals have salinities of 31.2%–41.5% $NaCl_{equ}$. This result reflects the characteristics of boiling fluid inclusions. In addition, the hydrogen and oxygen isotopic compositions ($\delta D_{v\text{-}SMOW}$ = −75 ‰ –−78 ‰, δO_{H2O} = 3.55 ‰ –3.85 ‰) show that the ore-bearing quartz veins in the skarns are closely related to magmatic-hydrothermal fluids (Fig. 11). The sulfur isotopic compositions ($\delta^{34}S$ = −2.2 ‰ –−0.1 ‰) of metal sulfides, including galena, chalcopyrite, tetrahedrite, and molybdenite, further confirm the source of magmatic sulfur. Therefore, it can be concluded that the skarns in the Jiama deposit originated from the metasomatism of magmatic-hydrothermal fluids. In the years following, Zhou Y et al. (2011) conducted an in-depth analysis of melt inclusions and fluid inclusions found in quartz, revealing that these inclusions have homogenization temperatures of 170–540°C, salinities of mostly 15%–50%, and densities of 0.9233–1.0805 g/cm^3. As revealed by Wang YY et al. (2017), the ore-forming fluids in the Jiama project is the NaCl-H_2O system. In combination with the inclusion compositions and the hydrogen and oxygen isotopic analysis, it can be determined that the ore-forming fluids are dominated by magmatic-hydrothermal fluids and could be mixed with meteoric water later. The decompression boiling and mixing of fluids might be important factors leading to the precipitation of the ore-forming fluids. However, the sulfur and lead isotopic analyses indicate that the sulfides (e.g., pyrite, galena, chalcopyrite, and molybdenite) in the skarns have $\delta^{34}S$ values of mostly −4.78 ‰ –0.83 ‰, which are comparable to those of the ore-

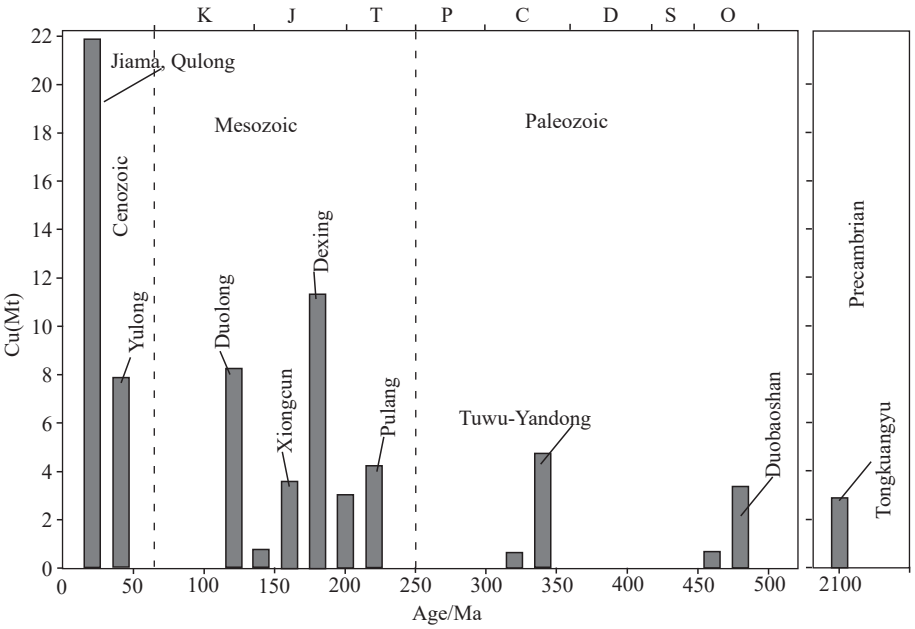

Fig. 10. Distribution of mineralization ages and tonnages of porphyry copper deposits in China (modified from Yang ZM et al., 2019).

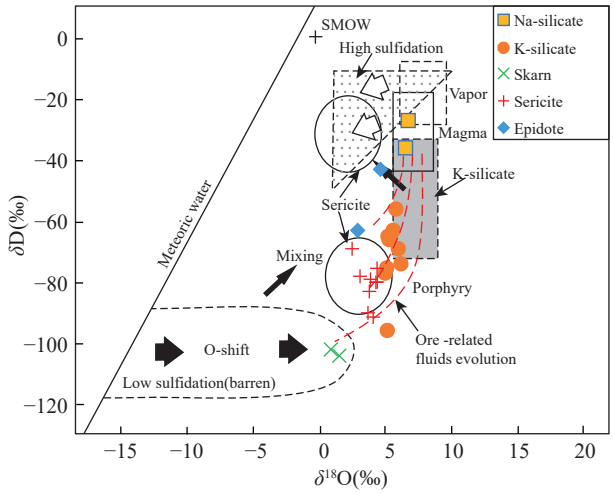

Fig. 11. Plot showing the hydrogen and oxygen isotopic compositions of different minerals in the Jiama deposit, Tibet (modified from Leng QF, 2016).

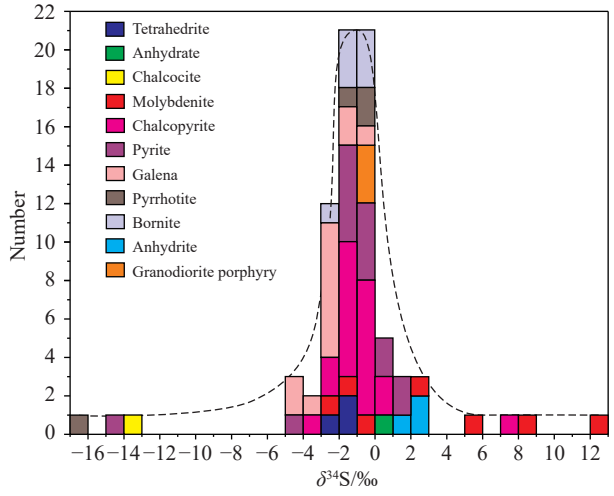

Fig. 12. Sulfur isotopic compositions of different minerals and rocks in the Jiama deposit, Tibet.

bearing granodiorite porphyry (−0.7 ‰ –0.2 ‰; Fig. 12). However, these sulfides have $^{206}Pb/^{204}Pb$, $^{207}Pb/^{204}Pb$, and $^{208}Pb/^{204}Pb$ ratios of 18.484–18.752, 15.547–15.638, and 38.058–39.740, respectively, which are consistent with the characteristics of the magmatic sulfur and mixed lead in orogenic belts (Zhou Y et al., 2012). In addition, Zheng WB (2012) and Guo WB et al. (2014) carried out a supplementary analysis of the H-O, S, and Pb isotopes in the Jiama project and systematically summarized the isotopic compositions mentioned above (Figs. 11–13; supplemetary Tables 1–3). The hydrogen and oxygen isotopic compositions of different stages of ore-bearing veins reflect the evolution of ore-forming fluids from magmatic-hydrothermal fluids to precipitation. Moreover, these isotopic compositions reveal that the fluids migrated from the intrusions on the No. 16 geological section, with the oxygen isotope values of the quartz veins tending to increase gradually. Based on the characteristics of the mineral assemblages (sulfides primarily, followed by sulfate minerals, and a small amount of anhydrite and gypsum locally) in the Jiama deposit, the sulfides have $\delta^{34}S$ values of mostly zero distributed in the form of a tower, reflecting the characteristics of magmatic sulfur. The pyrite, pyrrhotite, and chalcocite have some low $\delta^{34}S$ values (−16.8‰–−13.6‰), which may be related to the decrease in the number of the surrounding carbonaceous slates (Fig. 12). Furthermore, the lead isotopic compositions of metal sulfides and different ore-hosting rocks also imply that the lead in ore-forming fluids has a mixed source of orogeny and the lower crust (Fig. 13; Zheng WB, 2012).

Overall, the ore-forming fluids of the Jiama porphyry system were derived from magmatic-hydrothermal fluids rather than hydrothermal fluids in ancient oceans, as demonstrated by the characteristics of different types of fluid inclusions and H-O isotopic compositions in the Jiama project, as well as the sulfur and lead isotopic compositions of different metal minerals and rocks. The sulfur in the ore minerals were derived primarily from magmatic sulfur, which might be partially affected by the reduced sulfur from the surrounding carbonaceous rocks. Furthermore, the Pb reflects the mixed source of the orogeny and the lower crust and is controlled by the evolution of deep magmas.

5.3. Metallogeny and exploration models

Sillitoe RH (2010) has made a detailed summary of porphyry copper systems and constructed a general model, which effectively presents the spatial relationship of different types of orebodies in the same metallogenic system, as well as associated mineralization and alteration zones. This model has significant effects on the study and exploration of porphyry copper systems in a subduction setting (the circum-Pacific domain; Gatzoubaros M et al., 2014; Lin B et al., 2017). However, this model is based on the summary of subduction-related porphyry copper deposits and is not totally suitable for the porphyry copper systems in a collision setting (e.g., the Gangdese metallogenic belt; Wang R et al., 2018). Yang ZM et al. (2016, 2019) proposed that a collisional porphyry copper system differs significantly from a subduction-related porphyry mineralization system in terms of deep sources, magma evolution, and shallow alteration structure. Based on a case study of the Jiama deposit, Lin B et al. (2019) established a multi-center complex mineralization model for collision-related porphyry copper systems, summarized the basic geological elements and primary orebody types of collision-related porphyry copper systems, and identified differences between the model they established and the traditional porphyry model (Fig. 3).

The key differences between the porphyry copper systems in the Gangdese metallogenic belt and the traditional model are as follows: (1) Different tectonic backgrounds: the traditional model is suitable for a subduction environment (Cooke DR et al., 2005), while the Gangdese metallogenic belt was formed in a post-collisional extension environment (Hou ZQ et al., 2015; Wang R et al., 2018); (2) Different ore-hosting surrounding rocks: the traditional model has

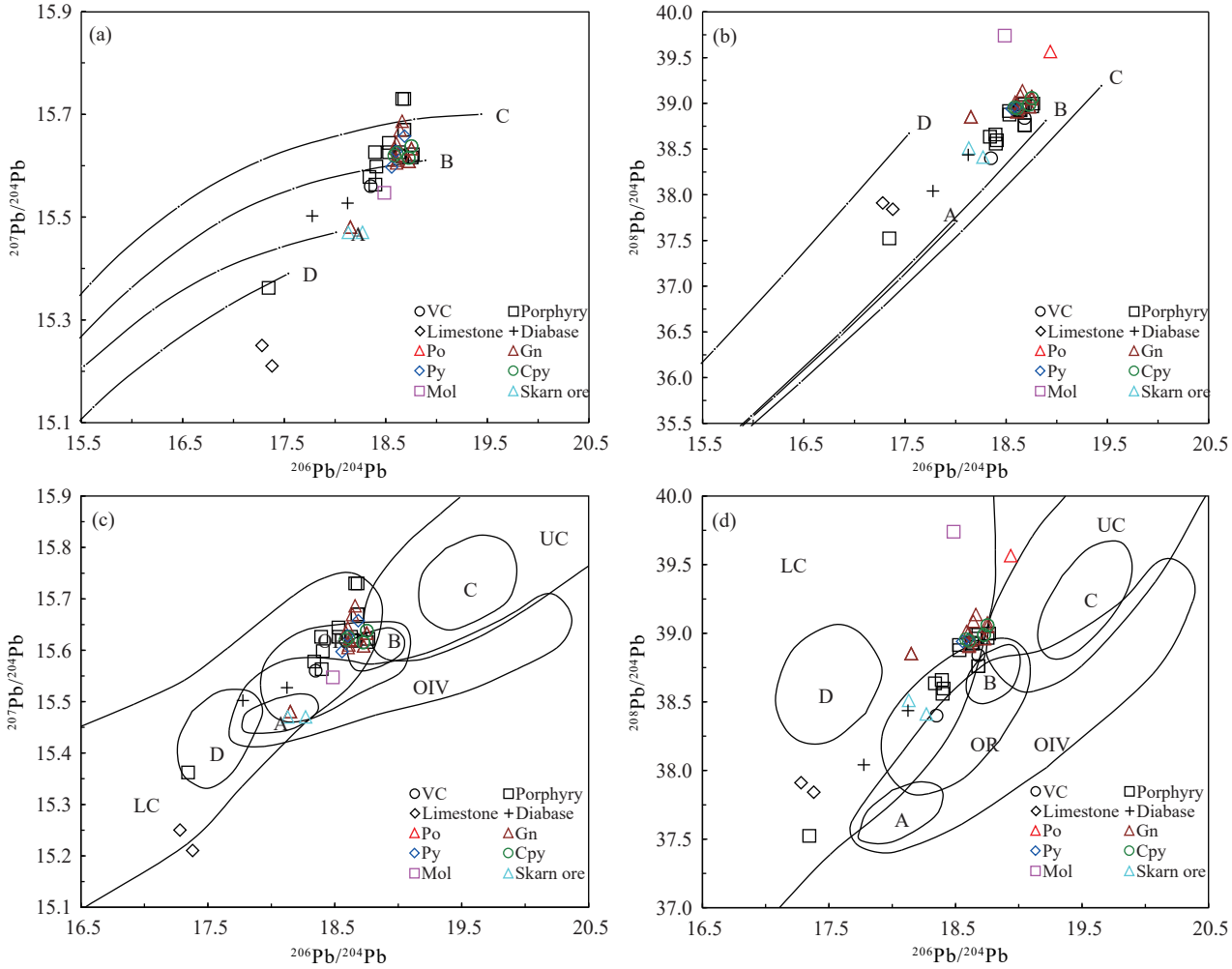

Fig. 13. Lead isotopic compositions of different rocks and minerals in the Jiama deposit (after Zartman RE and Doe B R, 1981; modified from Zheng WB., 2012). a–mantle, b–orogeny, c–upper crust, d–lower crust (Figs. a and b); UC–upper crust, LC–lower crust, OIV–ocean island volcanic rocks, OR–orogenic belt, a, b, c and d represent their central zones (Figs. c and d). Cpy–chalcopyrite; Gn–galena; Mol–molybdenite; Po–pyrrhotite; Py–pyrite; VC–volcanic rocks.

surrounding rocks dominated by Cenozoic calc-alkaline volcanic rocks, including andesite, dacite, and rhyolite (Harrison RL et al., 2018; Seedorff E et al., 2005), while the surrounding rocks of the porphyry copper systems in the Gangdese metallogenic belt primarily include Mesozoic marine sedimentary rocks (or clastics) and volcanic rocks (Lin B et al., 2012; Wang DH et al., 2011); (3) Different types of orebodies: compared with the traditional model, the porphyry copper systems found within the Gangdese belt host well-preserved porphyry-type orebodies and skarn orebodies, while almost entirely lacking epithermal orebodies; (4) Different hydrothermal centers: different types of mineralization are primarily concentrated in a single hydrothermal center in the traditional model, which fails to reveal the relationship between different hydrothermal centers. However, there are multiple hydrothermal centers in the Jiama giant porphyry deposit, and different hydrothermal centers can form multiple orebody structures (Lin B et al., 2019).

Based on the latest exploration and comprehensive studies of the Jiama project, the authors of this study have again represented a multi-center complex mineralization model for the Jiama porphyry copper system. Furthermore, by combining evidence from geology, mineralization and alteration structures, geochemical and spectral analyses, and indicator minerals, they built a comprehensive exploration model, aiming to provide a reference for future exploration and theoretical studies of porphyry copper deposit (Figs. 3, 14).

The multi-center complex mineralization model of the porphyry system can be described as follows: multi-stage intrusions, originating from the same shallow magma chamber and formed by magmatic evolution under a specific dynamical background (collision), intruded at different locations. After the emplacement of the intrusions, multi-stage fluids exsolved from a hydrothermal center and then formed porphyry, skarn, hornfels, independent gold, and/or epithermal orebodies and Manto-type orebodies during the evolution and precipitation of ore-forming fluids. In the process of mineralization and alteration, the hydrothermal centers at different locations related to different intrusions can be independent of each other, forming separate mineralization systems. Alternatively, they can be superimposed on each

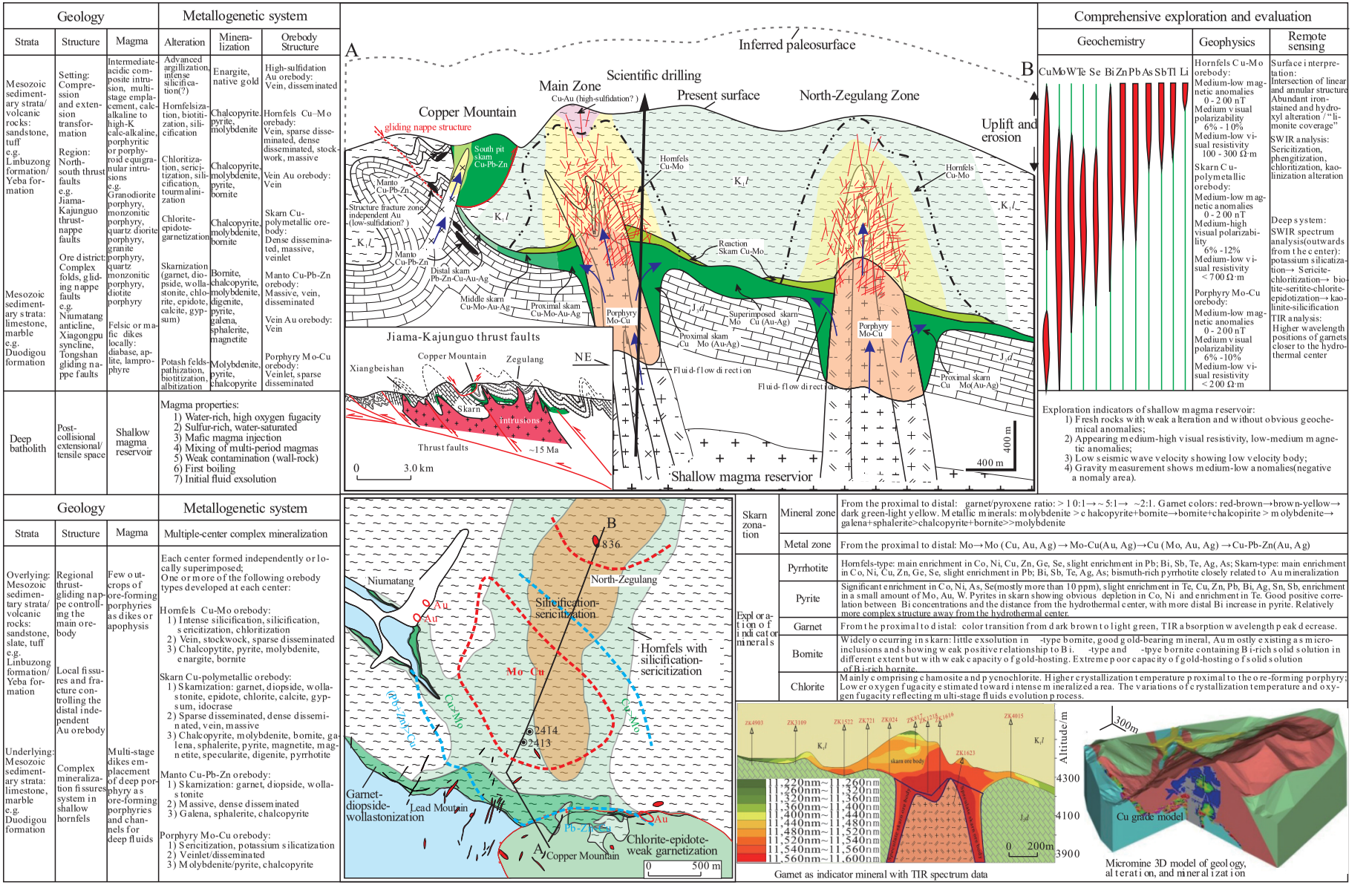

Fig. 14. Comprehensive exploration model of the Jiama deposit, Tibet.

other and form a complex mineralization system. During the formation of a superimposed metallogenic system, thick, large, and high-grade orebodies can be formed. In contrast, during the formation of a multi-center complex mineralization system, multi-stage magmatic-hydrothermal exsolution and evolution will form complex mineralization and alteration structures, as well as complex spatial zoning of ore-forming elements. Therefore, it is necessary to identify different hydrothermal centers and different mineralization stages in research on mineralization mechanisms and the exploration of multi-center complex mineralization systems. In the case of known giant porphyry copper systems, it is also possible to find more hydrothermal centers and other types of orebodies at their peripheries.

The comprehensive exploration model for the Jiama giant porphyry copper system mainly includes the basic geology, the structure of the metallogenic system, traditional exploration methods, and new exploration and evaluation technologies (Fig. 14; Lin B et al., 2019). The ore-forming geology and the structure of the metallogenic system are primarily interpreted planarly and vertically, aiming to obtain information such as the geology, structures, and igneous rocks of the Jiama porphyry copper system. This model also summarizes the mineral assemblages and their alteration features, along with the geochemistry of ore-related magmas. Traditional exploration methods in the model include geochemical and geophysical surveys and remote sensing surveys. The geochemical survey is mainly based on 1∶10000 soil and rock surveys on the surface of the project, as well as geochemical analysis of boreholes and the summary of the distributions of the Cu, Mo, W, Te, Se, Bi, Zn, Pb, As, Sb, Tl, and Ti anomalies (Halley S, 2015; Lin B et al., 2019; Zheng WB et al., 2021). The geophysical survey summarizes the magnetic and induced polarization characteristics of different types of orebodies, as well as the geophysical features used for identifying shallow magma reservoirs. Remote sensing surveys include regional analysis, as well as the analyses of short-wave infrared spectroscopy and thermal infrared spectroscopy of the Jiama project (Guo Na et al., 2019). The new exploration technologies and methods primarily include mineral zoning and the zoning of ore-forming elements for large skarn orebodies (Leng QF et al., 2022) and the investigation of various indicator minerals (Huang YR et al., 2021). The indicator minerals currently summarized include pyrrhotite, pyrite, garnet, bornite, and chlorite, and the details are as follows: (1) The pyrrhotite is primarily enriched in Co, Ni, Cu, Zn, Ge, and Se, followed by Pb, Bi, Sb, Ag, and As, and contains low contents of Mo, Cd, In, Sn, Ba, W, Au, Tl, Th, and U (Yang Y et al., 2020; Yang ZK et al., 2022). The origin of the gold-rich pyrrhotite in the skarns is closely related to Bi-bearing minerals (Yang ZK et al., 2022); (2) Determining the variations in the microstructure and Bi content of the pyrite help reveal the locations of the hydrothermal centers; (3) The change in the color of the garnet and the characteristics of the thermal infrared spectra show that a shorter distance from the hydrothermal center is associated with a darker color of the garnet and a longer thermal infrared wavelength (Hung YR et al., 2021); (4) The bornite can be further divided into multiple generations, has different trace element signatures, and is closely related to the gold-rich mineralization in the skarns; (5) The geochemistry of the chlorite can be used to indirectly calculate the temperature and oxygen fugacity of ore-forming fluids and then locate the hydrothermal center. Based on all the geological and exploration evaluation information mentioned above, a 3D model can be established using the Micromine or Leapfrog software. This aims to clearly display the spatial structure of the Jiama porphyry copper system and guide the exploration and mining of this system (Lin B et al., 2019; Tang P et al., 2017; Zheng WB et al., 2022). In addition, the National Key Research and Development Program conducted the first deep scientific drilling at a depth of 3 km in the Jiama project. This effort clearly revealed the metallogenic system's structure and provided key geological samples for understanding shallow magma reservoirs and mineralization mechanisms. Consequently, this contributed to the further improvement of the continental collision metallogeny and porphyry mineralization theories (Lin B et al., 2022).

6. Conclusions

(i) Jiama is the largest porphyry-skarn copper system in the Gangdese metallogenic belt and ranks first in China in order of the scale of skarn mineralization and copper resources. By the end of 2022, the Jiama project had discovered over 11×10^6 t of Cu, over 1.07×10^6 t of Mo, 1.75×10^6 t of Pb and Zn, 305 tons of associated Au, and 15840 t of associated Ag, making it a world-class giant deposit.

(ii) The Jiama porphyry copper system develops porphyry, skarn, hornfels, and independent gold orebodies, exhibiting complex alterations and mineralization structures. Its mineralization is closely related to Miocene intermediate-acidic magmatism. As confirmed by the fluid inclusions and the H-O, S and Pb isotopic analyses, the ore-forming fluids of the Jiama porphyry copper system originated primarily from magmatic-hydrothermal fluids and were later mixed with some meteoric water. The S and Pb in this system were derived mainly from deep magmas and a mixed source of orogeny and the lower crust, respectively.

(iii) The multi-center complex mineralization model of the Jiama porphyry system differs significantly from the traditional porphyry mineralization system in a subduction setting. A comprehensive exploration model has been jointly constructed for the system based on the geology, the structure of the metallogenic system, geochemistry, geophysics, remote sensing, spectral analysis, and the investigation of indicator minerals.

Credit authorship contribution statement

Bin Lin, Juxing Tang and Pan Tang conceived of the presented idea. All authors discussed the results and contributed to the final manuscript.

Declaration of competing interest

The authors declare no conflicts of interest.

Acknowledgements

This work was supported by the National Key Research and Development Program of China (2022YFC2905001), the National Natural Science Foundation of China (42272093, 42230813), China Scholarship Council project, and the Geological Survey project (DD20230054). We would like to thank these anonymous reviewers and editors for their constructive comments and input.

Supplementary appendix table

Supplementary data (Tables. S1–S3) to this article can be found online at doi: 10.31035/cg2023031.

References

Chung SL, Liu DY, Ji JQ, Chu MF, Lee HY, Wen DJ, Lo CH, Lee TY, Qian Q, Zhang Q. 2003. Adakites from continental collision zone: Melting of thickened lower crust in southern Tibet. Geology, 31, 1021–1024. doi: 10.1130/G19796.1.

Cooke DR, Hollings P, Walsh JL. 2005. Giant porphyry deposits: Characteristics, distribution, and tectonic controls. Economic Geology, 100, 801–818. doi: 10.2113/gsecongeo.100.5.801.

Duan JL, Tang JX, Mason R, Zheng WB, Ying LJ. 2014. Zircon U-Pb age and deformation characteristics of the Jiama porphyry copper deposit, Tibet: Implications for relationships between mineralization, structure and alteration. Resource Geology, 64, 316–331. doi: 10.1111/rge.12043.

Du GS, Yao P, Pan FC, Su DK, Li WB, Ning YY. 1998. Sedimentation-exhalation Skarn and its mineralization: An example from the Jiama Copper-polymetallic deposit, Tibet. Chengdu, Sichuan Science Publishing House. 82-113 (in Chinese).

Gatzoubaros M, Quadt AV, Gallhofer D, Rey R. 2014. Magmatic evolution of pre-ore volcanics and porphyry intrusives associated with the Altar Cu-porphyry prospect, Argentina. Journal of South American Earth Sciences, 55, 58–82. doi: 10.1016/j.jsames.2014.06.005.

Guo N, Cudahy T, Tang JX, Tong QX. 2017. Mapping white mica alteration associated with the Jiama porphyry-skarn Cu deposit, Central Tibet using field SWIR spectrometry. Ore Geology Reviews, 108, 147–157.

Guo WB, Zheng WB, Tang JX, Ying LJ, Wang YY, Lin B. 2014. Geochemical constraints on the source of metallogenic fluids and materials in the Jiama polymetallic Cu deposit, Tibet. Geology in China, 41(2), 510–528. doi: 10.3969/j.issn.1000-3657.2014.02.015.

Halley S, Dilles JH, Tosdal RM. 2015. Footprints: Hydrothermal alteration and geochemical dispersion around porphyry copper deposits. Economic Geology, 1, 12–17. doi: 10.5382/SEGnews.2015-100.fea.

Harrison RL, Maryono A, Norris MS, Rohrlach BD, Cooke DR, Thompson M, Creaser R A, Thiede DS. 2018. Geochronology of the Tumpangpitu porphyry Au-Cu-Mo and High-sulfidation epithermal Au-Ag-Cu deposit: Evidence for pre- and postmineralization diatremes in the Tujuh Bukit district, southeast Java, Indonesia. Economic Geology, 113, 163–192. doi: 10.5382/econgeo.2018.4547.

Hou ZQ, Duan LF, Lu YJ, Zheng YC, Zhu DC, Yang ZM, Yang ZS, Wang BD, Pei YR, Zhao ZD, McCuaig TC. 2015. Lithospheric architecture of the Lhasa Terrane and its control on ore deposits in the Himalayan-Tibetan orogen. Economic Geology, 110, 1541–1575. doi: 10.2113/econgeo.110.6.1541.

Hou ZQ. 2010. Metallogensis of continental collision. Acta Geologica Sinica, 84(1), 30–58 (in Chinese with English abstract).

Huang YR, Guo N, Tang JX, Shi WX, Ran FQ. 2021. Garnet characteristics associated with Jiama porphyry-skarn Cu deposit 1# skarn orebody, Tibet, using thermal infrared spectroscopy. Minerals, 11, 5. doi: 10.3390/min11010005.

Lang XH, Tang JX, Li ZJ, Huang Y, Ding F, Yang HH, Xie FW, Zhang L, Wang Q, Zhou Y. 2014. U-Pb and Re-Os geochronological evidence for the Jurassic porphyry metallogenic event of the Xiongcun district in the Gangdese porphyry copper belt, southern Tibet, PRC. Journal of Asian Earth Sciences, 79, 608–622. doi: 10.1016/j.jseaes.2013.08.009.

Large S, Wotzlaw, J, Guillong, M, von Quadt A, Heinrich C. A. 2020, Resolving the timescales of magmatic and hydrothermal processes associated with porphyry deposit formation using zircon U-Pb petrochronology. Geochronology, 2, 209–230. doi: 10.5194/gchron-2-209-2020.

Leng QF, Tang JX, Zheng WB, Lin B, Wang YY, Tang P, Lin X. 2015. A study of ore-controlling factors of thick and large skarn orebodies in Jiama porphyry metallogenic system, Tibet. Mineral Deposits, 34(2), 273–288 (in Chinese with English abstract). doi: 10.16111/j.0258-7106.2015.02.005.

Leng QF, Tang JX, Zheng WB, Tang P, Lin B. 2022. Skarn mineral assemblage and zonation pattern in the Jiama superlarge deposit, Tibet. Acta Geologica Sinica, 96(2), 574–591 (in Chinese with English abstract). doi: 10.19762/j.cnki.dizhixuebao.2021045.

Leng QF. 2016. Skarn diagenesis and metallogenesis in Jiama copper-polymetallic deposit, Tibet. Chengdu, Chengdu university of technology Ph. D thesis, 1–188 (in Chinese with English abstract).

Li GM, Rui ZY, Wang GM, Lin FC, Liu B, She HQ, Feng CY, Qu WJ. 2005. Molybdenite Re-Os dating of Jiama and Zhibula polymetallic copper deposits in Gangdese metallogenic belt of Tibet and its significance. Mineral Deposits, 24(5), 481–489 (in Chinese with English abstract). doi: 10.3969/j.issn.0258-7106.2005.05.002.

Li Y, Selby D, Condon D, Tapster, S. 2017. Cyclic magmatic-hydrothermal evolution in porphyry systems: High-precision U-Pb and Re-Os geochronology constraints on the Tibetan Qulong porphyry Cu-Mo deposit. Economic Geology, 112, 1419–1440. doi: 10.5382/econgeo.2017.4515.

Lin B, Tang JX, Chen YC, Song Y, Hall G, Wang Q, Yang C, Fang X, Duan JL, Yang HH. 2017. Geochronology and genesis of the Tiegelongnan porphyry Cu(Au) deposit in Tibet: Evidence from U-Pb, Re-Os dating and Hf, S, and H-O Isotopes. Resources Geology, 67, 1–21. doi: 10.1111/rge.12113.

Lin B, Tang JX, Zhang Z, Zheng WB, Leng QF, Zhong WT, Ying LJ. 2012. Preliminary study of fissure system in Jiama porphyry deposit of Tibet and its significance. Mineral Deposits, 31(3), 579–589 (in Chinese with English abstract). doi: 10.3969/j.issn.0258-7106.2012.03.015.

Lin B, Tang JX, Tang P, Zheng WB, Hall G, Chen GL, Zhang ZK. 2019. Polycentric complex mineralization model of porphyry system: A case study of Jiama superlarge deposit in Tibet: Mineral Deposits, 38(06), 1204–1222 (in Chinese with English abstract). doi: 10.16111/j.0258-7106.2019.06.002.

Lin B, Tang JX, Chen YC, Michael B., Song Y, Yang HH, Wang Q, He W, Liu ZB. 2019. Geology and geochronology of Naruo large porphyry-breccia Cu deposit in the Duolong district, Tibet. Gondwana Research, 66, 168–82. doi: 10.1016/j.gr.2018.07.009.

Lin B, Zhang XG, Pang P, Wang LQ, M. Santosh, Zha X, Zhang XX, Qi J, He L. 2021. Geology and geochronology of the Jinmuguo Mo polymetallic deposit: Implications for the metallogeny of the

Bangongco-Nujiang belt of Tibet. Ore Geology Reviews, 139, 104460. doi: 10.1016/j.oregeorev.2021.104460.

Lin B, Zou B, Tang P, He W, Liu ZY, Qi J, Li FQ, Chen L, Zhang XX, Sun M. 2022. Multiple isotopic dating constrains the time framework (Age) of a porphyry system: A case study from the Sangri Cu-Mo deposit, Bangongco-Nujiang metallogenic belt, Tibet, China, Ore Geology Reviews, 144, 104870. doi: 10.1016/j.oregeorev.2022.104870.

Lin B, Tang JX, Tang P, Georges B, Crystal F, Li FQ, Qi J, Zheng WB, Sun M, Cao HW, Song Y, Zou B, Zhou A, Leng QF, Yang C. 2023. Multi-pulsed magmatism and duration of hydrothermal system of the giant Jiama porphyry Cu system, Tibet, China. Economic Geology, under review.

Lin B, Wang LQ, Tang JX, Song Y, Cao HW, Baker M, Zhang LJ, Zhou, X. 2018, Geology, geochronology, geochemical characteristics and origin of Baomai porphyry Cu (Mo) deposit, Yulong Belt, Tibet. Ore Geology Reviews, 92, 186–204. doi: 10.1016/j.oregeorev.2017.10.025.

Li C, Qu WJ, Du AD. 2009, Decoupling of Re and Os and migration model of ^{187}Os in coarse-grained molybdenite. Mineral Deposits, 28, 707–712 (in Chinese with English abstract). doi: 10.3969/j.issn.0258-7106.2009.05.016.

Meng XY, Richards J, Mao JW, Ye HS, DuFrane S, Creaser R, Marsh J, Petrus J. 2020. The Tongkuangyu Cu deposit, trans-north China orogen: A metamorphosed Paleoproterozoic porphyry Cu deposit. Economic Geology, 115, 51–77. doi: 10.5382/econgeo.4693.

Pan GT, Mo XX, Hou ZQ, Zhu DC, Wang LQ, Li GM, Zhao ZD, Geng QR, Li ZL. 2006. Spatial-temporal framework of the Gangdese orogenic belt and its evolution. Acta Petrologica Sinica, 22(3), 521–533 (in Chinese with English abstract). doi: 10.3321/j.issn:1000-0569.2006.03.001.

Qi J, Tang JX, Lin B, Yang HR, Tang XQ, Tang P, Fang X, Zhang TT, Li FQ, Sun M, Wang MD, Xie JL. 2023. Geochronology, Geochemistry, and Implication of Aplite Dyke in the Giant Jiama Porphyry Copper System, Tibet. Acta Geologica Sinica - English Edition, doi: 10.1111/1755-6724.15037.

Qin ZP. 2013. Genetic model of the Jiama copper-polymetallic ore deposits, Tibet. Chengdu, Chengdu university of technology, Ph. D thesis, 1–167 (in Chinese with English abstract).

Qin ZP, Wang XW, Duo J, Tang XQ, Zhou Y, Peng HJ. 2011. LA-ICP-MS U-Pb zircon age of intermediate-acidic intrusive rocks in Jiama of Tibet and its metallogenic significance. Mineral Deposits, 30(2), 339–348 (in Chinese with English abstract). doi: 10.3969/j.issn.0258-7106.2011.02.014.

Sun F, Zhang JB, Wang R, Zhou LM, Jeon H, Li YY, Xue QW, Liu SY, Guo N, Luo CH, Xia WJ. 2022. Magmatic evolution and formation of the giant Jiama porphyry-skarn deposit in southern Tibet. Ore Geology Reviews, 145, 104889. doi: 10.1016/j.oregeorev.2022.104889.

Seedorff E. Dilles JH, Proffett JM, Einaudi MT, Zurcher L, Stavast WJA, Johnson DA, Barton MD. 2005. Porphyry deposits: Characteristics and origin of hypogene features. Economic Geology, 100, 251–298. doi: 10.5382/AV100.10.

She HQ. Feng CY, Zhang DQ, Pan GT, Li GM. 2005. Characteristics and metallogenic potential of skarn copper-lead-zinc polymetallic deposits in central eastern Gangdese. Mineral Deposits, 24(5), 508–520 (in Chinese with English abstract). doi: 10.3969/j.issn.0258-7106.2005.05.005.

She HQ, Feng CY, Zhang DQ, Li GM, Liu B, Li JW. 2006. Study on the fluid inclusions from Jiama skarn copper polymetallic deposit and Qulong porphyry copper deposit in Gandese copper belt, Tibet. Acta Petrologica Sinica, 22(3), 689–696 (in Chinese with English abstract). doi: 10.3321/j.issn:1000-0569.2006.03.018.

Sillitoe RH. 2010. Porphyry copper systems. Economic Geology, 105, 3–41. doi: 10.2113/gsecongeo.105.1.3.

Tang JX, Wang DH, Wang XW, Zhong KH, Ying LJ, Zheng WB, Li FJ, Guo N, Qin ZP, Yao XF, Li L, Wang Y, Tang XQ. 2010. Geological features and metallogenic model of the Jiama copper polymetallic deposit in Tibet. Acta Geoscientica Sinica, 31(04), 495–506 (in Chinese with English abstract). doi: 10.3975/cagsb.2010.04.02.

Tang JX, Deng SL, Zheng WB, Ying LJ, Wang XW, Zhong KH, Qin ZP, Ding F, Li FJ, Tang XQ, Zhong YF and Peng HJ. 2011. An exploration model for Jiama copper polymetallic deposit in Maizhokunggar county, Tibet. Mineral Deposits, 30(2), 179–196 (in Chinese with English abstract).

Tang JX. 2019. Mineral resources base investigation and research status of the Tibet Plateau and its adjacent major metallogenic belts. Acta Petrologica Sinica, 35(3), 617–624 (in Chinese with English abstract). doi: 10.18654/1000-0569/2019.03.01.

Tang JX, Lang XH, Xie FW, Gao YM, Li ZJ, Huang Y, Ding F, Yang HH, Zhang L, Wang Q, Zhou Y. 2015. Geological characteristics and genesis of the Jurassic No. I porphyry Cu –Au deposit in the Xiongcun district, Gangdese porphyry copper belt, Tibet, Ore Geology Reviews, 70, 438–456. doi: 10.1016/j.oregeorev.2015.02.008.

Tang JX, Duo J, Liu HF, Lang XH, Zhang JS, Zheng WB, Ying LJ. 2012. Minerogenetic series of ore deposits in the east part of the Gangdise metallogenic belt. Acta Geoscientia Sinica, 33(4), 393–410 (in Chinese with English abstract). doi: 10.3975/cagsb.2012.04.02.

Tang JX, Wang LQ, Zheng WB, Zhong KH. 2014a. Ore deposits metallogenic regularity and prospecting in the eastern section of the Gangdese metallogenic belt. Acta Geologica Sinica, 88(12), 2545–2555 (in Chinese with English abstract). doi: 10.3969/j.issn.0001-5717.2014.12.027.

Tang JX, Wang Q, Yang C, Ding S, Lang XH, Liu HF, Huang Y, Zheng WB, Wang LQ, Gao YM, Feng J, Duan JL, Song Y, Wang YY, Lin B, Fang X, Zhang Z, Yang YY. 2014b. Two porphyry-epithermal deposit metallogenic subseries in Tibetan Plateau: Practice of "absence prospecting" deposit metallogenic series. Mineral Deposits, 33(6), 1151–1170 (in Chinese with English abstract). doi: 10.3969/j.issn.0258-7106.2014.06.002.

Tang P, Tang JX, Zheng WB, Leng QF, Lin B, Tang X Q, Wang H, Gao X, Zhang ZB, Zhou HB. 2017. Is Tongshan orebody in the Jiama copper-polymetallic deposit Manto-type ore? Acta Geoscientica Snica, 38(5), 829–838 (in Chinese with English abstract). doi: 10.3975/cagsb.2017.05.21.

Tang P, Tang JX, Wang Y, Lin B, Leng QF, Zhang QZ, He L, Zhang ZB, Sun M, Wu CN, Qi J, Li YX, Dai SJ. 2021. Genesis of the Lakang'e porphyry Mo (Cu) deposit, Tibet: Constraints from geochemistry, geochronology, Sr-Nd-Pb-Hf isotopes, zircon and apatite. Lithos, 380–381, 105834. doi: 10.1016/j.lithos.2020.105834.

Tang P, Tang J X, Lin B, Zheng WB, Leng QF, Gao X, Zhang ZB, Zou B, Yang Y. 2019. The multi-factor constraints on the massive metallogenesis of porphyry ore-forming system-Case studies of Jiama superlarge deposit. Acta Petrologica Sinica, in press.

Wang DH, Tang JX, Ying LJ, Lin B, Ding S. 2011. Hornfels feature in the Jiama ore deposit, Tibet and its significance on deep prospecting. Acta Petrologica Sinica, 27(7), 2103–2108 (in Chinese with English abstract).

Wang R, Weinberg RF, Collins WJ, Richards JP, Zhu DC. 2018. Origin of postcollisional magmas and formation of porphyry Cu deposits in southern Tibet. Earth-Sciences Reviews, 181, 122–143. doi: 10.1016/j.earscirev.2018.02.019.

Wang YY, Zheng WB, Chen YC, Tang JX, Leng QF, Tang P, Ding S, Zhou Y. 2017. Discussion on the mechanism of seperation of copper and molybdenum in Jima porphyry deposit system, Tibet. Acta Petrologica Sinica, 33(2), 495–514 (in Chinese with English abstract).

Yao P. Li JG, Gu XX, Zheng MH, Chen JK. 2006. A discussion on the genesis of the stratabound skarn in the Jiama copper and polymetallic deposit of Tibet on the basis of REE and silicon isotope geochemistry. Acta Petrologica et Mineralogica, 25(04), 305–313 (in Chinese with English abstract). doi: 10.3969/j.issn.1000-6524.2006.04.006.

Yang ZM, Goldfarb RJ, Chang ZS. 2016. Generation of postcollisional porphyry copper deposits in southern Tibet triggered by subduction of the Indian continental plate. Special publication Society of Economic Geologist, 19, 279–300. doi: 10.5382/SP.19.11.

Yang ZM, Hou ZQ, White NC, Chang ZS, Li ZQ, Song Y C. 2009. Geology of the post-collisional porphyry copper –molybdenum deposit at Qulong, Tibet. Ore Geology Reviews, 36, 133–159. doi: 10.1016/j.oregeorev.2009.03.003.

Yang ZM, Cooke RD. 2019. Porphyry copper deposit in China. Economical Geology, SEG Special Publications, 22, 133−187. doi: 10.5382/SP.22.05.

Yang Y, Tang JX, Wu CN, Lin B, Tang P, Zhang ZB, He L, Qi J, Li YX. 2020. Typomorphic mineralogical characteristics of pyrrhotite in Jiama Cu polymetallic deposit, Tibet, and its geological significance. Mineral Deposits, 39(2), 337–350 (in Chinese with English abstract).

Yang ZK, Yang Y, Zhang ZK, Lin B, He J, Zhang ZB, Gao FT, Tang XQ, Tang P, Qi, J, Li YC. 2022. Geochemistry of pyrrhotite in the Jiama deposit, Tibet and its relationship with gold enrichment and precipitation. Geology in China, 49(4), 1198–1213 (in Chinese with English abstract). doi: 10.12029/gc20220411.

Yin A, Harrison TM. 2000. Geologic evolution of the Himalayan-Tibetan orogen. Annual Review of Earth and Planetary Sciences, 28, 211–280.

Ying LJ. 2012. The metallogeny of the Jiama copper polymetallic deposit in Tibet. Beijing, Chinese Academy of Geological Sciences, Ph. D thesis, 1–159 (in Chinese with English abstract).

Ying LJ, Tang JX, Wang DH, Chang ZS, Qu WJ, Zheng WB. 2009. Re-Os isotopic dating of molybdenite in skarn from the Jiama copper polymetallic deposit of Tibet and its metallogenic significance. Rock and Mineral Analysis, 28(3), 265–268 (in Chinese with English abstract). doi: 10.3969/j.issn.0254-5357.2009.03.014.

Ying LJ, Tang JX, Wang DH, Zheng WB, Qin ZP, Zhang L. 2011. Zircon SHRIMP U-Pb dating of porphyry vein from the Jiama copper polymetallic deposit in Tibet and its significance. Acta Petrologica Sinica, 27(7), 2095–2102 (in Chinese with English abstract).

Ying LJ, Wang DH, Tang JX, Chang ZS, Qu WJ, Zheng WB, Wang H. 2010. Re-Os dating of molybdenite from the Jiama copper polymetallic deposit in Tibet and its metallogenic significance. Acta Geologica Sinica, 84(8), 1165–1174 (in Chinese with English abstract).

Zartman RE, Doe BR. 1981. Plumb tectonics the model. Tectonophysics, 75, 135–162. doi: 10.1016/0040-1951(81)90213-4.

Zhang ZB, Tang JX, Tang P, Chen GL, Zhang ZK, Gao X, Yang Y. 2019. The origin of the mafic microgranular enclaves from Jiama porphyry Cu polymetallic deposit, Tibet: Implications for magma mixing/mingling and mineralization. Acta Petrologica Sinica, 35(3), 934–952 (in Chinese with English abstract). doi: 10.18654/1000-0569/2019.03.19.

Zheng, SJ, Zhong H, Bai ZJ, Zhang ZK, Wu CQ. 2021. High-sulfidation veins in the Jiama porphyry system, South Tibet. Mineralium Deposita, 56(2), 205–214. doi: 10.1007/s00126-020-00955-z.

Zheng WB, Tang JX, Zhong KH, Ying LJ, Leng QF, Ding S, Lin B. 2016. Geology of the Jiama porphyry copper–polymetallic system, Lhasa Region, China. Ore Geology Reviews, 74, 151–169. doi: 10.1016/j.oregeorev.2015.11.024.

Zheng WB, Liu BL, Tang JX, McKinley JM, Cooper MR, Tang P, Lin B, Li C, Wang L, Zhang D. 2022. Exploration indicators of the Jiama porphyry-skarn deposit, southern Tibet, China. Journal of Geochemical Exploration. 236, 106892. doi: 10.1016/j.gexplo.2022.106982.

Zheng WB, Tang JX, Wang XW, Wang H, Ying LJ, Zhong YF, Zhong WT. 2012. Analysis on gold metallization in Jiama copper polymetallic deposit, Tibet. Journal of Jilin University (Earth Science Edition), 42(1), 181−196 (in Chinese with English abstract).

Zhong KH, Li L, Zhou HW, Bai JG, Li W, Zhong WT, Zhang YQ, Lin JQ, Zheng FS, Huang XY, Lu B, Lei B. 2012. Features of Jiama (Gyama)-Kajunguo thrust-gliding nappe tectonic system in Tibet, Acta Geoscientia Sinica, 33(4), 411–423 (in Chinese with English abstract). doi: 10.3975/cagsb.2012.04.03.

Zhou Y, Wang XW, Tang JX, Qin ZP, Peng HJ, Li AG, Yang K, Wang H, Li J, Zhang JC. 2011. Origin and evolution of ore-forming fluids from Jiama copper polymetallic deposit in Tibet. Mineral Deposits, 30(2), 231–248 (in Chinese with English abstract). doi: 10.3969/j.issn.0258-7106.2011.02.006.

Zhou Y, Tang JX, Qin ZP, Peng HJ. 2012. Sulfur and lead isotope compositions and their geological implications of the Jiama copper polymetallic deposit. Metal Mine, 432(06), 102–105 (in Chinese with English abstract).

Zou B, Lin B, Zheng WB, Song Y, Tang P, Zhang ZB, Gao X. 2019. The characteristics of alteration and mineralization and geochronology of ore-bearing porphyry in south pit of Jiama copper-polymetallic deposit, Tibet. Acta Petrologica Sinica, 35(3), 953–967 (in Chinese with English abstract). doi: 10.18654/1000-0569/2019.03.20.